Chem Soc Rev

# When self-assembly meets biology: luminescent platinum complexes for imaging applications

| | |
|---|---|
| Journal: | *Chemical Society Reviews* |
| Manuscript ID: | CS-REV-12-2013-060453.R1 |
| Article Type: | Review Article |
| Date Submitted by the Author: | 14-Feb-2014 |
| Complete List of Authors: | De Cola, Luisa; Université Strasbourg, ISIS<br>Mauro, Matteo; université Strasbourg, ISIS<br>Aliprandi, Alessandro; université Strasbourg, ISIS<br>Septiadi, Dedy; université Strasbourg, ISIS<br>Kehr, Nermin; Westfaelische Wilhelms-Universitaet, Physikalisches Institut, Physikalisches Institut |
| | |

Journal Name

RSCPublishing

ARTICLE

# When self-assembly meets biology: luminescent platinum complexes for imaging applications

Cite this: DOI: 10.1039/x0xx00000x

Matteo Mauro,*[,a] Alessandro Aliprandi,[a] Dedy Septiadi,[a] Nermin Seda Kehr,[a] and Luisa De Cola*[,a]

Received 00th January 2012,
Accepted 00th January 2012

DOI: 10.1039/x0xx00000x

www.rsc.org/

Luminescent platinum complexes have attractive chemical and photophysical properties such high stability, emission in the visible region, high emission quantum yields and long excited state lifetimes. However the absorption spectrum of the compounds in the UV, preventing their excitation in the harmless visible/red region, as well as the strong quenching of the luminescent triplet state, caused by dioxygen in water and biological fluids, reduce their possible applications for imaging. Therefore a possible solution to these drawbacks is to take advantage of the high tendency of such square planar compounds to self-assembly in supramolecular structures. The assemblies can be considered a new chemical species with enhanced and tunable properties. Furthermore the assembly and disassembly process can be explored as a tool to obtain dynamic labels that can be applied in biomedicine. The change in color, the turn on and off of luminescence but also of the reactivity, the protection from quenching and environmental degradation, are some of the attractive properties connected to the aggregation of the complexes.

## 1. Introduction

In the last few decades, photoactive transition metal complexes (TMCs) have received a great deal of attention because of their rich and peculiar physico-chemical and redox properties. Particular interest has been devoted to second and third row transition metals with $d^6$, $d^8$ and $d^{10}$ electronic configuration, such as Ir(III), Ru(II), Os(II), Re(I), Pt(II), Pd(II), Ag(I) and Au(I),[1] as well as to the first row *e.g.* Cu(I),[2–5] and Zn(II). The presence of heavy metal atoms in TMCs introduces much more complicate, yet fascinating and unique, photochemical and photophysical attributes when compared to a general fluorescent organic molecule. Amongst all, judicious choice of metal ions and ligands yields to luminescent compounds, which show great photo- and electro-chemical stability, high photoluminescence quantum yield (PLQY), tunable emission color across the visible electromagnetic spectrum, from ultra-violet (UV) to near infra-red (NIR),[6–7] as well as long-lived emissive excited states. Indeed, as a consequence of the strong spin-orbit coupling (SOC) exerted by the heavy atom, intersystem crossing (ISC) processes yields to the population of energetically low-lying triplet excited states, and thus efficient radiative decay to the singlet ground state becomes allowed. Despite the triplet nature of the luminescent state emission quantum yield can, in some cases, approach 100%.[8]

Nowadays, growing interest on such photoactive TMCs is currently driven by their potential and real-market applications in optoelectronics,[9–10] photo-catalysis,[11–13] electrochemiluminescence (ECL),[14–15] metallogelators,[16] molecular devices,[17] non linear optical (NLO) materials,[18] spin-cross over (SCO),[19] components for electron and energy transfer systems,[20] bio-sensing,[21] and bio-imaging[22]. In very recent years, they emerged as promising candidates as active species in photonic devices which are attractive and powerful alternative to conventional lighting, such as energy-saving organic light-emitting diodes (OLEDs) and light-emitting electrochemical cells (LEECs),[23–29] as well as solar light harvesting materials for photovoltaic technology, such as in dye-sensitized solar cells (DSSCs).[30]

A growing and fascinating research field for luminescent TMCs is nowadays represented by their use as labels in bio-imaging application either *in vitro*, *in cellulo* or in the even more appealing *in vivo*. To date, some interesting reviews have been reported on the application of transition metals in luminescence cellular and bio-molecular imaging.[22,31–34] In addition, an excellent review has recently tried to rationalize the structure-cellular compartmentalization relationship, in order to achieve a better chemical design of such labels.[33] In this review, we focus our attention on phosphorescent platinum(II) complexes that have been in the last years successfully employed as luminescent labels for bio-imaging application. Even though Pt(II) complexes have been less investigated as bio-imaging probes compared to other metals such as Ir(III),[22] Ru(II),[35–36] Re(I),[37] and lanthanides-based complexes,[38–39] they possess attractive properties that octahedral $d^6$ and tetrahedral $d^{10}$ compounds do not. In fact, due to their square planar

geometry Pt(II) compounds exhibit a high stacking tendency resulting in the formation of assemblies. As it will be hereafter further discussed, this aggregation might blossom new avenues towards self-assembling of non-biological (or abiotic) entities into living systems. The assemblies might possess enhanced properties *e.g.* higher emission quantum yields, longer excited state lifetimes and reduced reactivity compared to the parental single components. Therefore, their use as imaging labels is very appealing for the preparation of novel hybrid materials or for the formation of nanostructures *within* cellular compartments. In particular, we will discuss how metallophilic interactions (*i.e.*, short closed-shell metal-metal interactions), which are favored by the geometry of these TMCs, can be advantageously used for bio-imaging purposes leading to a new class of labels with a potential in diagnostics and therapy. Indeed Pt(II) complexes have been extensively studied for cancer therapy,[40–42] but very few examples have shown the potentiality for theranostic applications so far. This new fascinating concept can be extended to other metal complexes which are able to provide sizeable metallophilic interactions, such as Au(I)-, Ag(I)-, Pd(II)-, Cu(I), Tl(I) and Hg(I)-based TMCs.[43–51]

## 2. General considerations

### 2.1 Basic photophysics of $d^8$ transition metal complexes

A number of excellent reviews and books have been already published describing in details the photochemistry and photophysics of TMCs, among which those based on $d^8$ metals, such as platinum(II). Hence, it is out of the scope of the present review to report on it, and the reader is kindly invited to refer to such papers.[52] However, for better following the forthcoming discussion, we wish to provide some basics concepts on the photophysics of square-planar $d^8$ platinum compounds.

As aforementioned, luminescent complexes possess a richer photophysics and photochemistry than most common organic chromophores. For TMCs, the presence of filled molecular orbitals with strong metal *d* character as well as of low-lying, empty, anti-bonding π* orbitals located on the ligands, yields to a more intriguing and lively photophysical scenario. This is primarily due to the energetic proximity of different electronic states and their different nature as well as to sizeable SOC effect exerted by the heavy atom. Unlikely common fluorescent organic molecules, the presence of heavy atoms in TMCs allows the mixing of the singlet and triplet manifolds due to SOC effects, which in a first approximation scales with the fourth power of the atomic number *Z* (SOC $\propto Z^4$), yielding to competitively fast ISC processes between electronic excited states of different multiplicity (*i.e.* singlet and triplet). For this reason, relaxation of the spin selection rules allows efficient radiative decay pathways from the lowest-lying excited state with mainly triplet character ($T_1$) to the singlet ground state ($S_0$), *i.e.* phosphorescence. Thermal relaxation of the excited molecule to its fundamental vibrational state within the $T_1$ electronic state gives rise to the typical large Stokes shift observed in luminescence TMCs. On the other hand, the partial permission of radiative deactivation channels, between states with mixed spin character, is responsible of the relatively slow excited state deactivation kinetics, which typically falls in the hundred of nanoseconds to tens of microsecond time scale.

Photoexcitation of such compounds with electromagnetic radiation occurring in the ultraviolet-visible (UV-VIS) region leads to the formation of excited states described, on the basis of their electronic transition configuration, as metal centred (MC), ligand centred (LC), interligand or ligand-to-ligand charge transfer (ILCT or LLCT), ligand-to-metal charge transfer (LMCT) and metal-to-ligand charge transfer (MLCT) (Fig. 1a). More precisely, upon optical excitation, such processes can be described as electron density redistribution between part of the molecules where filled and virtual orbitals with a certain nature are located. All the so far described features are typical of both $d^6$ and $d^8$ complexes.

Furthermore, the square-planar geometry of $d^8$ TMCs, such as platinum(II), yields to high tendency towards stacking, through establishment of ground-state intermolecular noncovalent weak metal···metal and/or ligand̃ligand interactions through the π-electron cloud of the aromatic rings.[46,53–61] In Fig. 1b is depicted the diagram of the molecular orbital closer to the frontier region for monomeric and two axial interacting platinum complexes. As shown, typical luminescent platinum compounds bearing strong field cyclometalating ligands as well as good π-accepting moieties, possess highest occupied and lowest unoccupied molecular orbitals, namely HOMO and LUMO, with dπ and $\pi^*$ character, respectively.

**Fig. 1**

On the basis of the ligand field (LF) theory, for a metal centre set in a square-planar arrangement of the coordinating ligands, relaxation of degeneracy of the *d* orbitals yields to filled $d_z^2$ orbital normal to the plane of the molecule, which does not (or only weakly) interact with the ligands' coordination sphere, and energetically lies below the HOMO level. The $d_z^2$ occupied orbital is thus prone to interact with surrounding species, as for instance solvent molecule (*e.g.*, dimethylsulfoxyde, namely DMSO) or neighbour platinum complexes. In the latter case, the formation of such ground-state metallophilic interaction, through the free axial position, destabilizes the filled $d_z^2$ orbitals, yielding a switch of the character of the HOMO level from dπ to σ* (*i.e.*, $d_z^2 \cdots d_z^2$). Owing to the Pt···Pt interaction, new excited-states are formed such as metal-metal-to-ligand charge transfer, namely MMLCT $^1(d\sigma^* \rightarrow \pi^*)$, and ligand-to-metal-metal charge-transfer (LMMCT). Interestingly, these charge transfer, CT, states typically show absorption and luminescence that are sizeably bathochromically shifted with respect to the parental, non-interacting, platinum complexes. It is important to note that the energy of such CT transitions strongly depends on the metal-metal distance, since the electronic interaction starts to occur at distance typically below 3.5 Å.

### 2.2 Self-assembly

### 2.2.1 Basics aspects

Self-assembly of smaller components into larger and more complex systems is an ubiquitous process that occurs at all levels: from the extremely large, such as galaxies, to the extremely small entities, such as molecules.[62] In general, self-assembly strongly engages with thermodynamics, and this allows the distinction between equilibrium and dissipative processes.[63–65] Even though the concept of self-assembly has been historically linked to biology, and in particular to biological structures such as cellular membrane and DNA, it has recently turned out to be a powerful and strategic tool in nanoscience.[66–68]

In such respect, life, in its deepest biochemical means, represents the ultimate, most complex and beautiful self-assembly process. The capability that indeed bio-molecules and bio-structures have to interact, recognize and self-replicate with incredibly high synchrony and low probability of error, plays a central role in life.

Nowadays, the possibility to design and chemically control long-range ordered nano- and micro-meter scale architectures, based on either organic or organo-metallic species, still represents a challenging research topic from both fundamental and applicative point of view.[67–69] Indeed, self-assembly through weak and noncovalent interactions has been shown to provide a way to organize molecules in supramolecular structures with properties superior to common bulk materials.

Several papers have already reported on the self-assembly in a competitive environment like water, while such supramolecular process is even more challenging *in cellulo* and *in vivo*. To date, inspiring examples of interaction between artificial structures and living systems were reported on the use of self-assembly of synthetic materials[70] as scaffold for directing cells behavior,[71] tissue regeneration[72] and blood vessels formation,[73] to cite some. On the other hand, beautiful examples of preparation of metallic and inorganic nanoparticles by using bio-templated and/or bio-directed self-assembly have been reported forming bio-hybrid materials.[74–77] Such very promising and fascinating examples have paved the way to self-assembly molecular components by means of weaker and non-covalent interactions in living cells.

To the best of our knowledge, only few examples are so far reported in which self-assembly of exogenous molecular (*i.e.*, organic and/or organometallic) components has been achieved in or triggered by very complicated environment such as living cells. In particular Rao and coworkers[78] have reported on the possibility to carry out a catalyzed condensation reaction under enzymatic control into living human cervical cancer cells, HeLa. The reported condensation process has been successfully visualized by means of fluorescence confocal imaging using a labeled biotin–streptavidin bio-conjugate. Moreover, Smith and coworkers[79] have nicely shown the possibility to form a host-guest system based on NIR-emitting squaraine–tetralactame macrocycle inclusion complexes with very high association constant. The complexation process has been easily followed by the increase of the NIR emission at *ca.* 700 nm even in high competitive biological environment such as bilayer membranes and in organelle with vesicle-like structures inside live Chinese hamster ovary (CHO) cells.

### 2.2.2 Self-assembly properties of luminescent platinum complexes

The possibility to prepare self-assembled nanostructures based on TMCs by means of supramolecular approaches represents an appealing topic with greatly growing interests.[80–81] This is due to the possibility to fabricate functional materials with emerging properties, compared to the bulk, by means of bottom-up approaches and it is driven by the potential advantage of the rich physico-chemical properties that metal complexes might possess. In particular, square-planar Pt(II) compounds with protruding filled $d_z^2$ orbitals have been known since long time to show high tendency towards stacking.

To date, it has been already reported that, in either organic or aqueous media, luminescent Pt(II) complexes are able to form homo-[82–83] and hetero-metallic[84–86] supramolecular architectures and superstructures as nanowires[87] nanosheets, nanowheels, nanotubes,[88] liquid crystals,[89] and metallogels[90–91] with very appealing (electro)optical,[92–94] sensing[95–96] and semiconducting properties.[97] Also, it has been nicely showed that the formation of such metallophilic interactions in luminescent square planar platinum complexes, and the subsequent modulation of their photophysical properties, can be induced by the presence of biological relevant molecules and poly-electrolytes in aqueous media.[95,98–100]

### 2.3 Emitters for imaging. Organic *vs* metal complexes.

Even though all the commercial cellular labels are based on organic fluorophores, luminescent metal complexes have a great potential for bio-imaging applications. There are several requirements that must be fulfilled in order to have a luminescent compound useful as a bio-imaging probe.

The compounds must be soluble and stable in aqueous media, such as phosphate buffered solution (PBS), cell culture media or in general the incubation media, as well as possess high cell permeability. Sometimes, addition of cell permeability agents, such as DMSO and low molecular weight alcohols at non-cytotoxic concentration level (<1% $^{v}/_{v}$), can also be employed in order to favour internalization. In particular, water solubility is not enough since the luminescent species must also possess a good degree of hydrophobicity to cross the phospholipidic cell membrane in order to be internalized. Therefore, amphiphilic complexes are desirable. As we will discuss in Section 3.2, such amphiphilic nature of the compounds can be successfully employed as tool for the preparation of self-assembled TMCs, which modulate their properties upon aggregation, as for instance luminescence and reactivity.

Following their internalization, the compounds should show high photochemical stability, low cytotoxicity, and produce no toxic products, at least on the time scale of the imaging experiments. However, such last requirement is often a drawback for photoactive TMCs, due to the fact that they show singlet oxygen ($O_2$ $^1\Delta_g$) sensitization upon photoirradiation, with relatively good quantum yields.[101–102]

Most of the bright luminescent TMCs display relatively intense ($\varepsilon \geq 10^3$ $M^{-1}$ $cm^{-1}$), but lower than the organic dyes, absorption bands in the UV-Vis range which can mainly be ascribed to singlet-manifold electronic transition with $^1$LC, $^1$ILCT and $^1$MLCT character. One of the advantages of luminescent complexes is their sizeable Stokes shift, mainly due to the energy gap between the absorbing singlet state and the triplet manifold responsible for the emission. Also the higher distortion of the emitting $T_1$ state, with respect to the optically excited one, further increases the degree of the shift. A large energy difference between excitation and emission spectra prevents secondary inner filter effects (*i.e.*, self-quenching) and interference with the emissive biomolecules. On the other hand, luminescent TMCs are strongly sensitive to dioxygen. The high emission quantum yields and the long excited state lifetimes (in organic deareated solvents) are strongly reduced in aereated aqueous media, and such issues are responsible for the rather rare use of TMCs as labels. Indeed, both the photophysical parameters are of great importance and need judicious attention. Noteworthy, the longer radiative deactivation kinetics allows the use of time-resolved and/or time-gated techniques, as for instance those based on lifetime imaging map (*i.e.* fluorescence lifetime imaging microscopy, FLIM). The combination of the large Stokes shift and long lifetime allows better energetic and temporal discrimination between emission arising from endogenous fluorophores (*i.e.*, auto-fluorescence) and the phosphorescent bio-label. The high emission quantum yield is desirable to allow a lower concentration of probe and a better visualization of the analysed substrate. Moreover, while designing molecules to be used for bio-imaging applications, one should keep in mind that UV light might damage biological specimens and the radiations have low transmittance. This is a major issue for thick specimens, as tissue, organs and even whole body (*in vivo*) imaging. On the other hand, tissues are relatively transparent at wavelengths in the range 600–1300 nm, called the optical therapeutic window. Molecules displaying relatively high two-photon absorption (TPA) cross-section or NIR absorption are therefore good candidates and in this respect metal complexes are key players. Furthermore red and NIR region is desirable for detection due to the lack of overlap with the fluorescence of biomolecules and the larger penetration of red light.

Finally, of great importance is where the labels are located inside cells. Indeed, cells possess distribution of organelles, membranes and structures, which are highly organized in terms of space, role and time. In such compartments, particular chemical reactions occur in a highly organized fashion, which allows vital cellular functions to take place. Seeking of luminophores able to imaging such compartments and, even more interesting, unravel bio-chemical reactions in real-time, plays a pivotal role in biological sciences. Thus, even though compartmentalization of bio-labels is still hard to predict, preventing a rational design of the emitters, it is desirable a targeting of specific sites. To this purpose, bio-conjugation of the luminophore has been widely used as a way to direct localization of the emissive compounds towards staining of specific organelle and compartments in both research stage and market products.

As it will be further illustrated and discussed, formation of metallophilic interactions, in aggregation-induced emission (AIE) active compounds, can constitute a valuable and clever way to both bathochromically shift absoption and emission spectra onset, while keeping high, or even enhancing, the photoluminescence quantum yield (PLQY). Also, protection from dioxygen or environmental quenching, maintaining long-lived excited state can be envisaged.

## 3. Luminescent Pt(II) complexes as bio-imaging labels

The potential and real applications of cyclometalated platinum(II) complexes in biology, which involves bio-labeling, cytotoxicity, phototoxicity and their ability to bind nucleic acids and proteins, have remained so far as one of the main reasons of very fast growing of research in the field of TMCs.[41]

The investigation of metal complexes for biological applications concerns almost always the compounds as monomeric species and rarely as in any aggregate form. This is despite the fact that aggregation could protect the metal complexes from interactions with the environment,[103] and allow the formation of species more stable towards chemical degradation. However, aggregation might give detrimental effects on the photophysical properties, such as emission quenching, *e.g.* through triplet-triplet annihilation (TTA), spectral broadening and, in some cases, formation of precipitate. So far, several strategies have been used in order to favor cell internalization and prevent their quenching by dioxygen and water molecules, such as caged complexes,[21,104] encapsulation in polymeric matrices, linking polyethylenglycol (PEG) moieties to the coordinated ligands,[105] increasing lipophilicity with long alkyl chains and bio-conjugation.[106–107] In particular, for platinum(II) complexes in either organic solvents or in solid state, self-assembled structures lead to changes in properties which are interesting and could be used to improve their use as labels. The ability to form aggregates is driven by the well-known tendency of square-planar platinum complexes to promote metallophilic interactions. We have recently reported that the aggregates exhibit enhanced luminescence properties,[92,108] and different emission colors depending on the packing.[91] Indeed, clever ligand design can allow the preparation of the emissive assemblies, where the photoluminescence properties of platinum compounds are even enhanced because of shielding effects imparted by the neighbor Pt(II) species (see cartoon in Fig. 2). Such protection yields to

**Fig. 2**

luminescent species which are almost insensitive to the environment and can therefore display high PLQY and excited-state lifetimes as long as in deareated conditions. Finally, it is worth to mention that assembling is a dynamic process and therefore the reversible formation of aggregates can be used to

 

following specific recognition event or localization of the complexes in certain organelles rather than others. All these emerging properties of the assemblies can be used for labeling and will be discussed in Section 3.2. In the next we will illustrate some selected examples of Pt(II) complexes used for imaging applications.

### 3.1 Non-assembled systems

Before discussing the self-assembly of square-planar platinum complexes, we are going to review some type of ligands that can be used to obtain luminescent systems and discuss how ligands can influence the fate of the compound in the cellular uptake. For these reasons, we have sorted the next section in three parts: the first dealing with the use of bidentate ligands; the second reporting tridentate-based derivatives, and a final section dealing with complexes in polymeric systems.

Many simple bi- and tri-dentate platinum(II) complexes, such as $[Pt(bpy)_2Cl_2]$, $[Pt(tpy)Cl]^+$ (where bpy and tpy are 2,2'-bipyridine and 2,2':6',2''-terpyridine, respectively) are usually either non-emissive or only very weakly luminescent at room temperature, due to the presence of low-lying MC (*d–d*) excited states, which are severely distorted compared to the ground state and hence subject to efficient non-radiative decay.[52] In order to increase the ligand field strength and raise the energy of the deactivating *d–d* states alternative routes have been reported. A possible solution is represented by the replacement of the monodendate chloride ligand(s) by a strong-field ligand as, for instance, an acetylide –C≡CR, leading to complexes that are emissive at room temperature. Alternatively, the polypyridyl ligand can be replaced by a cyclometalating analogue because of the very strong ligand-field induced by the cyclometalating carbon or negatively charged nitrogen, necessary to raise the energy of the deactivating *d–d* states. This approach has led to a variety of emissive complexes, including bidentate, tridentate and tetradentate chelates.[52] We have summarized all the major photophysical properties and their cell localization as well as their cytotoxicity in Table 1.

#### 3.1.1 Bidentate systems

***3.1.1.1 N^C systems***. Amongst bidentate ligands coordinated to platinum center in order to have luminescent species, the cyclometallated chelates are the most interesting ones because of their high stability and good emission properties. Despite the hundreds of complexes prepared and investigated with these ligands, only very few have been modified in order to have enough water solubility and to be exploited as bio-imaging label. All the chemical formulas of the relevant compounds are depicted in Chart 1. As a relevant example of this class of compounds, Lai *et al.*[109] reported a Pt(II) complex which was used for cell labeling and displays also photo-induced cytotoxicity. The cyclometalated compound depicted in Chart 1, namely $[Pt(thpy)(Hthpy)pyridine]^+$, **1**, where thpy is 2-(2'-thienyl)pyridine, shows a good absorption that extend to the visible region since the presence of $^1$MLCT Pt(5d) → π*(thpy) transitions. Complex **1** also exhibits room temperature orange emission with moderate emission quantum yield. The complex was reported to be uptaken by HeLa cells after incubation in culture media and to be predominantly localized inside the nucleus and the mitochondria. Interestingly, complex **1** showed noticeable toxicity under broadband visible light irradiation. Indeed, this complex, as many other metal

**Chart 1**

compounds, can sensitize oxygen by energy transfer, leading to the generation of toxic singlet oxygen.[21]

An interesting combination of imaging and toxicity which could lead to the development of this popular field, named theranostics, where diagnostics (in this case imaging) and therapy can be combined, was reported by Che and coworkers.[110] The authors described cyclometalated platinum(II) compounds, namely $[Pt^{II}(ppy)(bisNHC^{2C6})]OTf$, **2** (where ppy is 2-phenylpyridine and *bis*-NHC is a *bis*-*N*-heterocyclic carbene), and $[Pt^{II}(thpy)(bisNHC^{2C6})]OTf$, **3**, and their structures are shown in Chart 1. In this case, the authors showed that the reported green and orange emissive platinum complexes are strongly quenched by the buffer employed, as typical of most phosphorescent compounds. Nonetheless, addition of bovine serum albumin (BSA) allows protection of the complex from oxygen quenching and the emission intensity increases. The cellular uptake and toxicity of these two platinum(II) complexes were also reported. Upon internalization into HeLa cells, the authors claim selective staining of endoplasmic reticulum (ER) (Fig. 3) by their Pt(II)

**Fig. 3**

systems. Moreover, 3-(4,5-dimethylthiazol-2-yl)-2,5-diphenyltetrazolium bromide (MTT) assay experiments revealed very high toxicity activity for both complexes towards several cancer cell lines such as nasopharyngeal carcinoma (HONE1, SUNE1), breast cancer (MCF-7), lung carcinoma (HCC827, H1975), hepatocellular carcinoma (HepG2), and a non-tumorigenic liver cell line (MIHA). In particular, they reported that the toxicity of complex **3** was 5.3- to 60-fold stronger than cisplatin, a widely used drug for human cancers.[111] Moreover, they also explained that the toxicity activity was governed by the ER stress, inducing cell apoptosis.

Other examples of use of bidentate platinum(II) complexes in bio-imaging were reported by Huang and coworkers.[112] A series of four different membrane permeable compounds bearing β-diketonate ligands, namely **4–7,** are shown in Chart 1. It was reported that the luminescence properties were attributed to the mixing of $^3$MLCT, $^3$LLCT and $^3$LC/$^3$ILCT transitions. The influence of conjugation length on the energy levels of the β-diketonate ligands can vary excited state energies, thus the emission wavelengths can be tuned from 485 to 550 nm. The corresponding cellular uptake experiments are displayed in Fig. 4 and showed that the complexes were internalized into

**Fig. 4**

cytoplasmic region of the HeLa cells rather than merely staining the membrane surface. Interestingly, on the basis of MTT study, which showed more than 80% cell viability, it has been concluded that the complexes did not exhibit any toxicity activity, as compared with previous examples.

**TABLE 1**

***3.1.1.2 N^N systems.*** Besides N^C ligands, also N^N chelates coordinated to Pt ion have been investigated as potential labels. Mishra and coworkers reported on complex $[\{Pt(en)L\}_2]\cdot 4PF_6$, **8**, where $LH_2$ is *N*,*N'*-bis(salicylidene)-*p*-phenylenediamine and en is 1,2-diamino-ethane (see Chart 1 for the chemical structure).[113] The complex is internalized by HeLa cells and its toxicity evaluated by MTT assay study. Complex **8** was 2- and 10-fold more toxic than cisplatin towards HeLa and Dalton's Lymphoma (DL) cell lines, respectively. Co-localisation experiments with Hoechst, a fluorophore that bind the DNA inside the nucleus, are reported in Fig. 5. Such experiments

**Fig. 5**

confirmed the accumulation of the complex **8** inside the cells' nucleus and DNA binding was confirmed through the formation of the DNA-complex by means of UV-visible absorption spectroscopy. Indeed, calf thymus DNA (CT-DNA) in PBS, added to a solution of the platinum compound, causes a strong hyper-chromic shift by 30% of the absorption band at 254 nm and a small (3 nm) shift of the absorption band at 328 nm.

### 3.1.2 Tridentate systems

In order to meet one of the requirements for bio-imaging, *e.g.* chemical stability, an interesting chemical approach is to move from bidentate ligands to the corresponding tridentate chelates. A kinetic stabilization is indeed expected and the emission properties can also be retained using appropriate combination of C and/or N donor atoms in the conjugated coordinated ligands. Synthetic versatility and in particular introduction of asymmetry in the complex is also an advantage of such systems.[52]

***3.1.2.1 N^C^N systems.*** In order to gain deeper insights into the behavior of platinum complexes inside different type of cells, a very interesting class of compounds and spectroscopic tools have been described by Williams and coworkers.[114–115] They reported on highly emissive and photostable platinum(II) species of general formula [PtLCl], namely **9**, where HL is 1,3-di(2-pyridyl)benzene. The introduction of substituents on the central ring resulted in different derivatives, **9a–b** (Fig. 6). In their work it has been demonstrated that the green luminescent complexes possess microsecond lifetimes and emission quantum yields of up to 70% in organic solvents and deareated conditions, which are exceptionally high for platinum complexes. After an incubation time as short as 5 minutes, the two complexes **9a–b** are internalized in a range of live cell lines, such as normal human dermal fibroblast (HDF), neoplastic C8161 and CHO, with apparently diffusion controlled uptake kinetics and negligible up to low toxicity. Due to their low absorption in the visible region, a NIR two-photon excitation was employed to excite the platinum systems. The exceptional long excited state lifetime of the complexes allowed the author to apply an interesting time-gated technique to eliminate fluorescence background or emission coming from other cell labels.

This technique represents a nice tool to discriminate localization of the complex inside the cell but also to gain insights onto the environment to which the platinum is exposed. The change in the excited-state lifetime depending on the different localization of the complex inside the cell has been more recently demonstrated,[115] since the same authors have shown that they can map the excited state decays inside the cells by applying a new powerful method of "two-photon time-resolved emission imaging microscopy" (TP-TREM). The method combines microsecond-range imaging with enhanced multi-photon resolution and allows time-resolved detection on a timescale of several orders of magnitude longer than that available in FLIM, yet maintaining the essential sub-μm spatial resolution afforded by two-photon excitation techniques. They apply this novel technique on the first water-soluble representative of the family of probes **9b** (Fig. 6), since the

**Fig. 6**

previous study was made with **9a** that was less water-soluble. Complex **9b** shows a two-photon absorption, TPA, with a cross-section as high as 3.5 GM at 760 nm. Remarkably, likely for other derivatives of the family **9**, no photo-bleaching has been detected under intense prolonged irradiation. The TP-TREM method produces simultaneously information on the energy, intensity and decay time of the emission in tridimensional (3D) spatial resolution. The lifetime map gives interesting insights on the surrounding environment of the Pt complex **9b**, since the excited state decay kinetics decreases moving from the cell membrane ($\tau$ ~300 ns), to the cytoplasm ($\tau$ ~4.2 μs) and finally into the nucleus ($\tau$ ~5.8 μs) (Fig. 6). However, at this stage, the authors cannot rule out the cleavage of the coordinated $Cl^-$, and thus, there is no clear evidence of the exact nature of the emissive species and what type of surrounding the luminophore experiences. Furthermore, interaction of the complex with biomolecules can create a shielding microenvironment, which can be accounted for the preservation of the good emitting properties of the platinum species. The changes in the first or second coordination sphere and/or a more hydrophobic or rigid environment provide a variable degree of protection from quenching by oxygen, with subsequent decrease of the non-radiative pathways kinetics. Indeed the authors demonstrated that an interaction between the DNA and the complex might occur, as evidenced by the enhancement of the emission intensity when the complex is

 

treated with CT-DNA and salmon sperm DNA in aqueous phosphate or HEPES buffer in the presence of NaCl.

***3.1.2.2 C^N^N systems.*** The change of the position of the cyclometallated ring from a central to a lateral location yields to complexes with very different spectroscopical properties. As discussed in recent reviews and papers.[116–119] the general trend shows reduced emission quantum yield accompanied by shorter excited-state lifetime. This change in the spectroscopic properties does not prevent the use of such complexes as cell-imaging probes.

Lam and coworkers reported on a series of organometallic platinum(II) complexes with a new tridentate cyclometalating ligand 2-phenyl-6-(1*H*-pyrazol-3-yl)pyridine and its derivatives, which contains a $C_{phenyl}$^$N_{pyridyl}$^$N_{pyrazolyl}$ chromophoric moiety.[120] The chemical structure of the complex **10**, is reported in Table 1. As for many platinum complexes, the absorption in the visible is very limited and the authors overcome such a problem using two-photon excitation to populate the emissive excited state. The compound exhibits intense green emission under ambient conditions with a structured emission profile in the region 500–520 nm (see Table 1 for details). HeLa and NIH3T3 cells were incubated with complex **10** for various time durations (0–60 minutes). At an exposure time of 5 minutes, more than 95% of the cells exhibited green luminescence but no clear images of the localization of the compound have been reported. However, the authors claimed an even localization throughout the cytoplasmic region. Cytotoxicity of **10** towards HeLa and NIH3T3 cells was also tested by means of MTT assay. Upon 6 hours exposure of cells to complex **10** at a 20-fold higher concentration respect to the dose used for imaging experiments, the measured viability was similar to that of the control tests. This low level of cytotoxicity of **10** is consistent with that observed by Botchway *et al.*[114] in the series of complexes **9** on CHOK1 animal-derived cell line. Emission spectra of **10** internalized by HeLa and NIH3T3 cells were recorded by means of a confocal microscopy and compared with the emission profile in solution. Due to the similarity of the spectra, the authors concluded that the nature of the emission arising from the cyclometalated platinum complex **10** before and after entering the cells is similar and the lost of fine structure for the profile recorded into the cells tentatively attributed to the different environment (organic solvent *vs* cellular environment, respectively). However, it has not been ruled out the possibility that the measured broad and featureless emission band centered at *ca.* 520 nm arose from the cellular endogenous auto-fluorescence due to flavin adenine dinucleotide (FAD),[121–122] rather then the platinum complexes.

Derivatization of 2-phenyl-6-(1*H*-pyrazol-3-yl)pyridine by incorporation of an hydrophobic $C_{18}$ chain and replacement of the ancillary chloride ligand by a water soluble *p*-trisulfonated triphenylphosphine ($[PPh_3\text{-}3SO_3]^{3-}$) have led to an anionic water-soluble complex, $[Pt(L_2)(PPh_3\text{-}3SO_3)]^{2-}$, namely **11**, with interesting amphiphilic characteristics and closely resembling anionic surfactants such as sodium dodecyl sulfate, SDS.[123] The corresponding chemical structures are reported in Fig. 7.

**Fig. 7**

The cyclometalated complex **11** shows a strong absorption features in the range 300–400 nm and weaker transitions at lower energies. The higher donating ability of the $SO_3$-substituted $PPh_3$ moiety pushes the lower-lying MLCT transition to higher energies, causing the overlapping of the $^1$MLCT absorption bands with the $^1$IL states. Upon excitation at 355 nm at room temperature in aqueous media (HEPES buffer at pH 7.0), complex **11** displayed a poorly resolved emission in the green region (see Table 1 for details). Also, derivate **11** displayed poor absorption features in the visible range, and the authors succeeded with the two-photon excitation of the sample at $\lambda_{exc}$ = 720 nm, reproducing exactly the same emission band. Likewise its parent complex **10**, complex **11** was rapidly taken up and accumulated in HeLa cells at a dosage as low as 1 μg $mL^{-1}$. However, the authors report that the cells were not washed after incubation with the complex. Due to the long hydrophobic $C_{18}$ carbon chain, compound **11** showed rapid and efficient localization in the plasma membrane of live cells and the *p*-trisulfonated triphenylphosphine ancillary ligand is also believed to help maintaining the localization of the complex in the plasma membrane. MTT viability assay experiments performed on HeLa cells and normal epithelial cells showed values up to 90% and 70% cell viability after 25 hours of exposure, respectively.

In order to localize the platinum complexes in different part of cells, Koo *et al.* synthesized a platinum(II)compound bearing a (triphenyl{5-[3-(6-phenylpyridin-2-yl)-1*H*-pyrazol-1-yl]pentyl}phosphonium chloride) as cyclometalating ligand,[124] **12**, and its chemical structure is shown in Table 1. The presence of a terminal cationic triphenylphosphonium moiety as a bioactive pendant should induce a preferential localization since it is known that this functionalization often delivers different bioactive molecules to mitochondria both *in vitro* and *in vivo*.[125–126] Spectroscopic properties of complex **12** resembled those of its related compound **10**. In $CH_3CN$ at 298 K, complex **12** gives a slightly structured profile and relatively low emission quantum yields (see Table 1).

Unlikely its parental complex **10** which was claimed to evenly stain the cytoplasmic region, upon excitation at 405 nm, characteristic emission of **12** was detected in both nuclei and cytoplasm of HeLa and 3T3 cells with some nuclear domains strongly enriched, and weak cytoplasmic background (Fig. 8).

**Fig. 8**

Indeed, complex **12** accumulated rapidly in living HeLa cells, with nucleoli clearly labeled within 15 minutes of incubation. Significant degree of cell death was observed for different cell lines 4 hours later. Complex **12** was also found to be a potent inhibitor of transcription. Even though it did not show any nucleic acids binding properties, its nuclear staining behavior

may be mediated by specific interactions with some nuclear or nucleolar proteins.

The derivatization of the C^N^N ligands with carboxylic acid was investigated by Che and coworkers.[127] The chemical structure of the most representative [Pt(C^N^N)Cl] complexes is sketched in Fig. 9. The compounds showed solubility and stability in aqueous solutions at room temperature and ability to bind to proteins via non-covalent interaction.

Excitation of **13a–b** at $\lambda$ = 410 nm gave a weak emission at 563 and 522 nm, respectively whereas, **14**–**15** exhibited a weak

**Fig. 9**

emission at 656 nm in DMSO/$H_2O$ and 631 nm in $H_2O$, respectively. Interestingly, even though solution of **13** (60 μM) in PBS was weakly emissive, the addition of bovine serum albumin (BSA) resulted in up to a 26-fold increase in emission intensity upon increase from 0 to 1.0 of concentration ratio of [BSA]/[**13a**] (Fig. 9). Noteworthy, changing the additive from BSA to glycine, phenylalanine, or tryptophan did not result in any emission enhancement, not even at a 10-fold molar ratio of the amino acid *vs* complex **13a**.

After 5 minutes incubation of HeLa cells with **13a** the complex was internalized and a marked enhancement of luminescence was observed within 24 hours. The bright field image of HeLa cells after incubation with **13a** showed that the complex mostly distributed inside the cytoplasm, with a lower level of nuclear uptake. However, the higher degree of localization of the complex in the perinuclear region made the author suggest that **13a** interacts with organelles such as the ER and Golgi apparatus. Also, toxicity studies showed that complex **13a** is relatively non-cytotoxic towards HeLa cells with $IC_{50}$ of 80 μM.

In order to enhance stability against biological reduction and ligand exchange reactions, Sun *et al.* reported on C^N^N-based platinum(II) complexes bearing N-heterocyclic carbene (NHC), as the ancillary ligands, namely **16**–**18**, and their structure is depicted in Fig. 10a.[128] Contrarily to closely related

**Fig. 10**

previously reported cyclometalated Pt(II) complexes, but analogously for the carbene containing bidentate systems, complexes **16**–**18** show highly cytotoxic and specificity towards cancerous cells.

Apart from the good solubilty in organic solvents, they showed to be stable in water and, more importantly, resistance towards reduction/substitution by glutathione (GSH). The mononuclear complexes **16a**–**d**, **17a–b** are emissive in the solid state and in degassed $CH_3CN$ with very similar emission $\lambda_{max}$ at around 545 nm with moderate emission quantum yields. The dimeric specie **18f** displays a more red shifted emission with maximum at 619 nm.

Complex **16a** (Table 1) was internalized by HeLa cell and, even more importantly, displayed promising anti-cancer activity towards several cancer cell lines ($IC_{50}$ = 0.057–0.77 μM). Notably, this complex is less cytotoxic to the normal-derived human cell line (CCD-19Lu) with $IC_{50}$ value of 11.6 mM, which is 232-fold higher than for HeLa cells. To ascertain the site of cellular localization, cells previously incubated with **16a** were further co-stained with known fluorescent dyes and the majority of **16a** can be co-localized with MitoTracker (Fig. 10).

Moreover, Che and coworkers described two Pt(II) allenylidene complexes supported by tridentate cyclometalated ligands having mixed N- and C-donor atoms, and the corresponding structures are depicted in Fig. 11.[129] These metal–allenylidene complexes exhibit many intriguing

**Fig. 11**

functionalities including self-assembled nanostructures and biological activity.

Solutions of complexes **19a** and **19b** in $CH_2Cl_2$ are yellow with a modest low-energy absorption band at $\lambda_{max}$ = 400 nm. When the concentration of **19a** in $CH_2Cl_2$ is increased above $2\times10^{-5}$ M, an additional distinct absorption band emerges at $\lambda_{max}$ = 440 nm. The latter band is tentatively ascribed to a $^1$MMLCT transition derived from molecular aggregates through Pt···Pt interactions. The absence of MMLCT absorption band in the case of **19b** is attributed to the two bulky *tert*-butyl groups disfavoring intermolecular stacking interactions in solution. Upon excitation at around 400 nm, Pt(II) complexes **19** –**b** in dilute degassed $CH_2Cl_2$ solutions show intense yellow-green emission.

The combination of a planar cationic structure and intriguing phosphorescent properties renders these metal allenylidene complexes possible switching probes for DNA molecules in aqueous solutions. The authors demonstrated that a 17- and 5-fold enhancement in intensity was observed upon addition of DNA for **19a** and **19b**, respectively. They also investigated the applications of these complexes in cell imaging. HeLa cells were incubated with either **19a** or **19b**. Observation under a fluorescence microscope revealed living cell morphologies with **19a** predominately localized in the nucleus whereas **19b** mainly accumulated in the cytosolic region (Fig. 11). The bulky *tert*-butyl groups in **19b** may impede deep intercalation of **19b** into DNA and prevent its localization into the nucleus. The *in vitro* cytotoxicity of the complexes towards HeLa cells was evaluated by using the MTT assay, which showed $IC_{50}$ values of 5.8 and 9.0 μM after 48 hours incubation for **19a** and **19b**, respectively, and turned out to be more cytotoxic than cisplatin ($IC_{50}$ = 19 μM in the control experiment).

Besides cell imaging platinum complexes have also been employed to detect specific metal ions. In this respect Zhang *et al.* explored the use of platinum(II) complex in the field of two-photon probes for $Hg^{2+}$ ion detection bearing a tridentate 6-phenyl-2,2'-bipyridine (C^N^N) and the corresponding structures is sketched in Fig. 12.[130] The novel water-soluble

**Fig. 12**

C^N^N-Pt(II)–alkynyl complex, namely **20,** was designed in such a way to display two-manifold features. On one hand, the

 

introduction of a rhodamine derivative as functional pendant moiety allowed the well-known mercury-promoted desulfurization reaction and spirolactam ring opening process, triggering the fluorescence to turn-on. On the other hand, the C^N^N-Pt(II)–alkynyl moiety increased nonlinear absorption properties of the employed system. Thus, the compound is expected to be helpful for estimation of trace amounts of mercury ions in live cells by means of two-photon microscopy.

Among the various metal ions, the chemosensor **20** displayed highly selective color changes and fluorescent increase upon the addition of $Hg^{2+}$ (Fig. 12b). The detection limit was determined by fluorescence enhancement and estimated to be $4.87\times10^{-7}$ M in $CH_3CN$ and HEPES buffer. The authors also demonstrated that the high sensitivity towards mercury in the presence of other competitive species. The same photophysical behavior was also observed inside HeLa cells. Two-photon microscopy image cells labeled with **20** showed weak luminescence, presumably due to the efficient fluorescence quenching by photo-induced electron transfer (PET). The presence of Hg ions, added to the solution, was clearly revealed by an increase in the emission intensity (Fig. 12 c–d).

***3.1.2.3 N^N^N-binding ligands.*** Wu and coworkers reported a new fluorescent system, namely **21**,[131] constructed by tethering a fluorophore, 4-amino-7-nitro-2,1,3- benzoxadiazole (4-amino-NBD), to a tridentate chelate, BPA (*N*,*N*-bis(pyridin-2-ylmethyl)amine]), able to coordinate a Pt ion (Fig. 13a).

**Fig. 13**

Both the ligand and the complex **21** can be internalized inside different cells lines. Interestingly the authors report that the free ligand is localized in the cytoplasmic region (Fig. 13b) while the complex is also observed in the nucleus (Fig. 13c). After 4−5 h of incubation it is however not clear if the migration of the complex inside the nucleus is induce by the fact that the cells became swollen, which is a common appearance for cell paraptosis. Complex **21** in different cell lines showed lower cytotoxicity than cisplatin in human pulmonary carcinoma cell (A549), breast carcinoma (MCF-7), and ovarian cancer cell lines (COC1 and CAOV3), see Table1.

### 3.1.3 Encapsulation of platinum complexes in confined matrices

An important approach to shift the absorption and emission of the platinum complexes in the red part of the electromagnetic spectrum has been pioneered, for imaging applications, by Tanke and co-workers.[132] They have developed two compounds with general formula Pt meso-tetra (4-carboxyphenyl)porphine (PTP), namely **22** and Pt 3,8,13,18-tetramethyl-21*H*,23*H*-porphine-2,7,12,18-tetrapropionic acid (PTCP), namely **23** see Table 1. The complexes derivatives, PTP-*N*-hydroxysuccinimide (PTP-NHS) and PTCP-*N*-hydroxysuccinimide ester (PTCP-NHS ester) were successfully used to label avidin derivatives as well as some antibodies. Interestingly, the authors showed internalization of their compounds in HeLa cells and, with such red long-lived emitting species, proved that time gated emission can be successfully used to overcome the autofluorescence problems of the biosystems.[133]

A further improvement on the properties of porphyrinic systems has been recently described by Prasad and coworkers.[134] It is well known that encapsulating metal complexes inside polymeric particles or micelles,[103,135] could prevent oxygen quenching avoiding decreasing of luminescence intensity in air-equilibrated media. The combination of encapsulation and red emissive platinum(II) complex was realized with a Pt(II)-tetra-phenyltetranaphthoporphyrin, namely **24**, entrapped in PEG-modified phospolipid micelles and its structure is sketched in Fig. 14a. Complex **24** showed

**Fig. 14**

very interesting photophysical properties, such as maximum absorption at 691 nm and the emission peak at 903 nm in $CHCl_3$ solution (Table 1). Interestingly, the average decay time for **24** was found to increase three-fold after the encapsulation. In addition, quantum yield also increased up to 30% upon confinement. These observations confirm the ability of polymeric micelles to hinder access to oxygen molecules.

The toxicity study was carried out with pancreatic cancer cell line Panc-1 (ATCC, CRL-1469) and showed slight, dose-dependent toxicity of the nanomicelles over a period of 24 h. Interestingly, as shown in Fig. 14b–d, *in vivo* study in nude mice with pancreatic tumor xenografts reveals distribution of the complex-micelles inside the tumor tissue and liver 96 hours after the injection.

Another Pt(II) complex, namely **25** (Fig. 15), which has

**Fig. 15**

been protected by the environment by embedding it into polyacrylamide-coated poly-styrene, to form polymeric luminescence particles, was reported by Huang and coworkers.[136] The complex shows no emission in any solvents, but unexpectedly shows very intense emission in crystal state (PLQY up to 38%) which has been ascribed to the a restriction of distortion of excited state structure mechanism. The enhanced emission of **25** was maintained in the polymeric structure (Fig. 15a) and in order to increase water solubility and cell uptake the particles were functionalized with folic acid and incubated with HeLa cells. As shown in Fig. 15, the hybrid materials seemed to accumulate only inside cytoplasm and cytotoxicity study showed no toxicity even after 24 hours of incubation, with cell viability of 95% (see Table 1).

## 3.2 Assembled systems

As discussed above, platinum(II) complexes can in some cases aggregate into dinuclear,[57,118,137–138] trinuclear,[52,118,137] or even multinuclear[87,108] arrays through formation of (extended) metallophilic and π–π interactions. As far as luminescence

TMCs is concerned, aggregation has been since long time considered more a drawback, mostly due to the concomitant decrease of PLQY, a phenomenon generally called aggregation caused quenching (ACQ). Moreover, severe decrease of solubility and color purity can be also envisaged upon aggregation. On the other hand, very recently an increasing interest has been devoted to design and preparation of luminophores showing opposite effects, *i.e.* phenomena known as aggregation induced emission (AIE) and aggregation induced emission enhancement (AIEE).[139] So far, few fascinating examples of conjugated organic, and TMCs based on Ir(III),[140] Pt(II),[92,108] and Re(I)[141] have been reported. Furthermore, the advantage to have and/or induce formation of TMCs aggregates, in particular based on Pt complexes, can be manifold and might lead to: *i*) shielding of the emitter from the environment and in particular from dioxygen to avoid quenching and/or formation of toxic species;[103,134] *ii*) rigidochromic effect due to the packing of the molecules in fixed structures, causing decreasing of non-radiative processes;[136] *iii*) switch-off of reactivity or toxicity caused by the isolation of complexes and difficult accessibility of the metal center; *iv*) changes in the excited state nature and/or properties leading to bathochromic shift of both excitation and emission towards more biologically interesting spectral windows, such as red and NIR region. All these features are more difficult to be achieved by using octahedral complexes, such as Re(I), Ru(II) and Ir(III) derivatives, and would definitely constitute great advantages for bio-imaging applications.

To this purpose, we have recently investigated on the self-assembly as a tool to obtain luminescent nanostructures based on neutral tridentate platinum(II)[108] complexes also in cellular compartments[142]. Our group has preliminarily demonstrated that the platinum complexes showed in (Fig. 16–17), namely **26**, **Tol-Pt-4OHpy** and **27**, **$CF_3$-Pt-4OHpy**, respectively, are internalized in living cells and they self-assemble into nanosized aggregates. The choice of the coordinated ligands was dictated by the interest in forming neutral and amphiphilic complexes. The nature of the substituents on the tridentate ligand changes the HOMO–LUMO properties, leading to different energies of the exited states of the complexes, as well as a different lipophilicity and size of the systems. It is indeed known in medicinal chemistry that $CF_3$ groups enhance cell and nuclear permeability, while lipophilicity generally enhance cellular uptake even though being responsible of increased cytotoxicity.[143-144]

**Figs. 16 and 17**

The compounds have remarkable photophysical properties with emission in the green and blue region for **26** and **27** respectively, in solid state. In solution their properties depends dramatically on the concentration and on the employed solvent. In water:1% v/v DMSO, both complexes are present in an aggregate form displaying an intense yellow emission arising from $^3$MMLCT transitions. Noteworthy, the assemblies under excitation are bright emitters, with long-lived triplet excited-state lifetimes, even in the presence of oxygen, and enhanced photostability. Complex **26** and **27** are both internalized into HeLa cells within few minutes, and demonstrate how the choice of the coordinating ligands can determine the aggregates formation preferentially into the cytoplasmatic region, Fig. 16 and in the nucleus, Fig. 17, for **26** and **27** respectively. Both the complexes possess the same emission in water:1% v/v DMSO and after cell uptake, as clearly shown in Fig. 16–17, suggesting that the compounds are in the aggregate form inside the cell. At this stage we cannot say if the complexes are uptaken as aggregates or as monomeric species and aggregate subsequently in the cell. The most striking results are with complex **27** since it is able to localize into the nucleoli as proven by colocalization experiments performed by using Phalloidin Alexa Fluor® 568, 4',6-diamidino-2-phenylindole-6-carboxamidine (DAPI) and SYTO® RNASelect™ Green Fluorescent Cell Stain, for staining of actin, nucleus and nucleoli, respectively. The corresponding confocal microscopy pictures are shown in Fig. 18 and clearly confirm that the bright

**Fig. 18**

aggregates emission is coming from the nucleoli and the cytoplasm. Interestingly, the excited state decay kinetics measured by confocal fluorescence lifetime imaging microscopy (FLIM) displays a multi-exponential decay with one of the components being as long as 920 ns for the stained nucleoli. Even more importantly, the aggregation process through (extended) ground-state $d_{z2}\cdots d_{z2}$ metallophilic interactions leads to $^1$MMLCT state. The establishment of such lower-lying state nicely allowed excitation of the labels with wavelengths up to 543 nm, as shown in Fig. 19. As already mentioned the aggregates display

**Fig. 19**

an enhanced photostability which is also observed inside the cell, after strong excitation with a Hg lamp irradiation at 365 nm for several minutes up to one hour, while the DAPI emission is photobleached after few minutes.

The concept of assembly and disassembly of aggregates to be used as dynamic labels for cell imaging has been recently proved by Yam and coworkers.[145] The authors reported a series of water-soluble alkynylplatinum(II) terpyridine complexes **28** (Fig. 20a) that can aggregate and disassemble over changes in pH which are in the physiological range, resulting in drastic emission intensity changes in the NIR region (Fig. 20b) and

**Fig. 20**

evidenced by dynamic light scattering (DLS). The trigger for the changes in the aggregation properties is the acidity of phenolic proton of the complex **28a** which at high pH increase the hydrophilicity of the complex and hence its deaggregation in aqueous medium. The emission of the complex is present only when the compound is in the aggregate form at pH

between 3.5 and 5.6. Above 5.6 in pH the NIR emission shows a significant drop in intensity and becomes completely "turned-off" at or above pH 7.6 (Fig. 20b). In addition, the complete "turning-off" of the NIR emission of complex **28a** at high pH, suggest a combination of aggregation/deaggregation of platinum(II) complex moieties and PET that would be energetically more favourable to occur in basic solution, probably due to the deprotonation of the phenolic groups on the alkynyl ligand of complex **28a** which becomes more electron-rich. This has further been supported by a lack of pH-dependence of the NIR emission of an aqueous solution of the control complex, **28c**, at 788 nm.

Confocal microscopy images of fixed MDCK cells incubated with complex **28a** in serum and phenol red free Dulbecco's modified Eagle's medium (DMEM) revealed a strong NIR emission band in vesicular distribution (Fig. 20c). The MDCK cells remained viable after the incubation (MTT assay result ca. 97% viability as compared to untreated MDCK cells) and showed good co-localization, with the green emission of LysoSensor Green DND-189, in acidic organelles such as lysosomes.

## 4 Conclusion and outlook

The research presented in this review clearly indicated that the use of metal complexes and in particular of luminescent Pt(II) systems is an important and relative young field in bio-imaging. So far however problems related to the intrinsic properties of the complexes, e.g. the lack of visible absorption bands for low energy excitation (partially overcame by two photon techniques), the quenching by dioxygen and biomolecules, low solubility in water, prevent their full exploitation as biolabels. In addition, the relationship between their chemical structures and cell uptake, localization and toxicity remains elusive.

The planar geometry would favor the formation of aggregates, which in the case of Pt(II) complexes can result in assemblies possessing high stability and interesting photophysical properties. Such aggregates can be indeed considered a new class of dynamic probes, since the luminescence can be turned on and off but also the emission color, the excited state lifetime and quantum yield can be modulated by assembling or disassembling the system. Their dynamic behavior can be envisaged to investigate not only the visualization of certain parts of the cell or tissues, but also to explore chemical recognition event or biochemical reaction. A clever design of the complexes can in fact lead to the realization of assemblies sensitive to *e.g.* pH or polarity of the environment, oxygen content, formation of redox species, so that their change in emission color, in size or even their migration from one part of the cell to other sites can be related to cellular chemical changes. These visionary previsions are not far to be realized since in two of the examples reported here, it is clear that the assemblies can be obtained in living cells and therefore they can be reporters of subtle intracellular changes.

## Acknowledgements

The authors kindly acknowledge University of Strasbourg, CNRS, the LabEx "Chemistry of Complex Systems", and the Ministère de l'Enseignement Supérieur de la Recherche (MESR) and ERC grant n. 2009-247365 for financial support. L.D.C. is grateful to the Région Alsace and the Communauté Urbaine de Strasbourg for the award of a Gutenberg Excellence Chair (2011-2012) and to AXA Research funds.

## Notes and references

[a] Laboratoire de Chimie et des Biomatériaux Supramoléculaires, Institut de Science et d'Ingénierie Supramoléculaires (I.S.I.S.) – UMR 7006 Université de Strasbourg, 8 allée Gaspard Monge, F-67083 Strasbourg (France) Fax: +33 (0) 3 6885 5242; Tel: +33 (0) 3 6885 5220; E-mail: mauro@unistra.fr; decola@unistra.fr.

† Footnotes should appear here. These might include comments relevant to but not central to the matter under discussion, limited experimental and spectral data, and crystallographic data.

Electronic Supplementary Information (ESI) available: [details of any supplementary information available should be included here]. See DOI: 10.1039/b000000x/

1 See dedicated issue V. Balzani, S. Campagna (Eds.) *Top. Curr. Chem.*, 2007, **280–281**.
2 A. Barbieri, G. Accorsi, N. Armaroli, *Chem. Commun.*, 2008, **19**, 2185–2193.
3 D. V. Scaltrito, D. W. Thompson, J. A. O'Callaghan, G. J. Meyer, *Coord. Chem. Rev.*, 2000, **208**, 243–266.
4 A. L. Cambot, M. Cantuel, Y. Leydet, G. Jonusauskas, D. M. Bassania, N. D. McClenaghana, *Coord. Chem. Rev.*, 2008, **252**, 2572–2584.
5 D. R. McMillin, J. R. Kirchhoff, K. V. Goodwin, *Coord. Chem. Rev.*, 1985, **64**, 83–92.
6 N. Darmawan, C.-H. Yang, M. Mauro, M. Raynal, S. Heun, J. Pan, H. Buchholz, P. Braunstein, L. De Cola, *Inorg. Chem.*, 2013, **52**, 10756–10765.
7 M. S. Lowry, S. Bernhard, *Chem. Eur. J.*, 2006, ***12***, 7970–7977.
8 Y. Kawamura, K. Goushi, J. Brooks, J. J. Brown, H. Sasabe, C. Adachi, *App. Phys. Lett.*, 2005, **86**, 071104–071107.
9 M. Panigati, M. Mauro, D. Donghi, P. Mercandelli, P. Mussini, L. De Cola, G. D'Alfonso, *Coord. Chem. Rev.*, 2012, **256**, 1621–1643.
10 P.-T. Chou, Y. Chi, *Chem. Eur. J.,* 2007, **13**, 380-395.
11 M. S. Lowry, J. I. Goldsmith, J. D. Slinker, R. Rohl, R. A. Pascal, G. G. Malliaras, S. Bernhard, *Chem. Mater.*, 2005, **17**, 5712–5719.
12 S. Rau, D. Walthera, J. G. Vos, *Dalton Trans.*, 2007, **9**, 915–919.
13 R. Reithmeier, C. Bruckmeier, B. Rieger, *Catalysts*, 2012, **2**, 544–571.
14 M. Staffilani, E. Holss, U. Giesen, E. Schneider, F. Hartl, H. P. Josel, L. De Cola, *Inorg. Chem.*, 2003, **42**, 7789–7798.
15 M. M. Richter, *Chem. Rev.*, 2004, **104**, 3003–3036.

16 A. Y.-Y. Tam, V. W.-W. Yam *Chem. Soc. Rev.*, 2013, **42**, 1540–1576.
17 V. Balzani, M. Venturi, A. Credi (Eds.) *Molecular Devices and Machines*, Wiley-VCH, 2006.
18 S. Di Bella, *Chem. Soc. Rev.*, 2001, **30**, 355–366.
19 M. A. Halcrow (Ed.) *Spin-crossover materials: properties and applications*, Wiley, 2013.
20 P. Ceroni, V. Balzani *Photoinduced energy and electron transfer processes* in *The exploration of Supramolecular systems and nanostructures by photochemical techniques* P. Ceroni (Ed.), Springer, 2012.
21 A. Ruggi, F. W. B. van Leeuwen, A. H. Velders, *Coord. Chem. Rev.*, 2011, **255**, 2542–2554.
22 V. Fernández-Moreira, F. L. Thorp-Greenwood, M. P. Coogan, *Chem. Commun.*, 2010, **46**, 186–202.
23 H. Yersin (Ed.) *Highly Efficient OLEDs with Phosphorescent Materials*, Wiley-VCH, Weinheim, Germany, 2008.
24 M. E. Thompson, P. E. Djurovich, S. Barlow and S. Marder, *Organometallic Complexes for Optoelectronic Application*s, in *Comprehensive Organometallic Chemistry III*, ed. R. H. Crabtree and D. M. P. Mingos, Elsevier, Oxford, UK, 2006.
25 C. Cebrián, M. Mauro, D. Kourkoulos, P. Mercandelli, D. Hertel, K. Meerholz, C. A. Strassert, L. De Cola, *Adv. Mater.*, 2013, **25**, 437–442.
26 M. Mauro, C.-H. Yang, C.-Y. Shin, M. Panigati, C.-H. Chang, G. D'Alfonso, L. De Cola, *Adv. Mater.*, 2012, **24**, 2054–2058.
27 M. Mydlak, C. Bizzarri, D. Hartmann, W. Sarfert, G. Schmid, L. De Cola, *Adv. Funct. Mater.*, 2010, **20**, 1812–1820.
28 R. D. Costa, E. Ortí, H. J. Bolink, F. Monti, G. Accorsi, N. Armaroli, *Angew. Chem. Int. Ed.*, 2012, **51**, 8178–8211.
29 T. Hu, L. He, L. Duan, Y. Qiu, *J. Mater. Chem.*, 2012, **22**, 4206–4215.
30 B. E. Hardin, H. J. Snaith, M. D. McGehee, *Nature Photonics*, 2012, **6**, 162–169.
31 K. K.-W. Lo, A. W.-T. Choi, W. H.-T. Law, *Dalton Trans.*, 2012 **41**, 6021–6047.
32 E. Baggaley, J. A. Weinstein, J. A. G. Williams, *Coord. Chem. Rev*., 2012, **256**, 1762–1785.
33 Q. Zhao, C. Huang, F. Li, *Chem. Soc. Rev.*, 2011, **40**, 2508–2524.
34 K. K.-W. Lo, K. Y. Zhang, S. P.-Y. Li, *Pure Appl. Chem.*, 2011, **83**, 823–840.
35 C. A. Puckett, J. K. Barton, *J. Am. Chem. Soc.*, 2007, **129**, 46–47.
36 M. R. Gill, J. A. Thomas, *Chem. Soc. Rev.*, 2012, **41**, 3179–3192.
37 R. G. Balasingham, M. P. Coogan, F. L. T. Greenwood, *Dalton Trans.*, 2011, **40**, 11663–11674.
38 C. P. Montgomery, B. S. Murray, E. J. New, R. Pal, D. Parker, *Acc. Chem. Res*. 2009, **42**, 925-937.
39 B. Song, C. D. B. Vandevyver, A. S. Chauvin, J. C. G. Bünzli, *Org. Biomol. Chem.*, 2008, **6**, 4125–4133.
40 E. Chardon, G. Dahm, G. Guichard, S. Bellemin-Laponnaz, *Organometallics*, 2012, **31**, 7618–7621.
41 For a recent review: T. C. Johnstone, J. J. Wilson, S. J. Lippard, *Inorg. Chem.*, 2013, **52**, 12234–12249.
42 F. Arnesano, M. Losacco, G. Natile, *Eur. J. Inorg. Chem.*, 2013, **15**, 2701–2711.
43 V. Vreshch, W. Shen, B. Nohra, S. K. Yip, V. W.-W. Yam, C. Lescop, R. Réau, *Chem. Eur. J.*, 2012, **18**, 466–477 and refs therein.
44 V. W.-W. Yam, E. C.-C. Cheng, *Chem. Soc. Rev.*, 2008, **37**, 1806-1813.
45 V. W.-W. Yam, K. K.-W. Lo, *Chem. Soc. Rev.*, 1999, **28**, 323–334.
46 J. Muñiz, C. Wang, P. Pyykkö, *Chem. Eur. J.*, 2011, **17**, 368–377.
47 L. H. Doerrer, *Dalton Trans.*, 2010, **39**, 3543–3553.
48 J. Lefebvre, R. J. Batchelor, D. B. Leznoff, *J. Am. Chem. Soc.*, 2004, **126**, 16117–16125.
49 U. Patel, H. B. Singh, G. Wolmershuäser, *Angew. Chem. Int. Ed.*, 2005, **44**, 1715–1717.
50 A. J. Goshe, I. M. Steele, B. Bosnich, *J. Am. Chem. Soc.*, 2003, **125**, 444–451.
51 M. J. Mayoral, C. Rest, V. Stepanenko, J. Schellheimer, R. Q. Albuquerque, G. Fernandez, *J. Am. Chem. Soc.*, 2013, **135**, 2148–2151.
52 See for instance: J. A. G. Williams, *Top. Curr. Chem.*, 2007, **280,** 205–268.
53 V. H. Houlding, V. M. Miskowski, *Coord. Chem. Rev.,* 1991, **111**, 145–152.
54 V. M. Miskowski, V. H. Houlding, *Inorg. Chem.*, 1991, **30**, 4446–4452.
55 C. A. Strassert, M. Mauro, L. De Cola, *Adv. Inorg. Chem.* 2011, **63**, 48–103.
56 I. M. Sluch, A. J. Miranda, O. Elbjeirami, M. A. Omary, L. M. Slaughter, *Inorg. Chem*, 2012, **51**, 10728–10746.
57 B. Ma, J. Li, P. I. Djurovich, M. Yousufuddin, R. Bau, M. E. Thompson, *J. Am. Chem. Soc.*, 2005, **127**, 28–29.
58 D. Kim, J. L. Brédas, *J. Am. Chem. Soc.*, 2009, **131**, 11371–11380.
59 M. Kato, C. Kosuge, K. Morii, J. S. Ahn, H. Kitagawa, T. Mitani, M. Matsushita, T. Kato, S. Yano, M. Kimura, *Inorg. Chem.*, 1999, **38**, 1638–1641.
60 H. B. Gray, A. W. Maverick, *Science*, 1981, **214**, 1201–1205.
61 G. Gliemann, H. Yersin, *Struct. Bonding*, 1985, **62**, 89–150 and refs therein.
62 G. M. Whitesides, B. A. Grzybosky, *Science*, 2002, **295**, 2418–2421.
63 C. A. Palma, M. Cecchini, P. Samorì, *Chem. Soc. Rev.*, 2012, **41**, 3713–3730.
64 B. A. Grzybowsky, A. H. Stone, G. M. Whitesides, *Nature*, 2000, **405**, 1033–1036.
65 B. A. Grzybowsky, C. E. Wilmer, J. Kim, K. P. Browne, K. J. M. Bishop, *Soft Matter*, 2009, **5**, 1110–1128.
66 G. M. Whitesides, J. P. Mathias, C. T. Seto, *Science*, 1991, **254**, 1312–1319.
67 J. M. Lehn, *Science*, 2002, **295**, 2400–2403.
68 D. N. Reinhoudt, M. Crego-Calama, *Science*, 2002, **295**, 2403–2407.
69 R. F. Service, *Science*, 2001, **293**, 782–785.

 

70 S.-W. Lee, C. Mao, C. E. Flynn, A. M. Belcher, 2002, *Science*, **296**, 892–895.
71 J. D. Hartgerink, E. Beniash, S. Stupp, *Science*, 2001, **294**, 1684–1688.
72 T. Dvir, B. P. Timko, D. S. Kohane, R. Langer, *Nature Nanotech.*, 2011, **6**, 13–22.
73 K. Rajangam, H. A. Behanna, M. J. Hui, X. Han, J. F. Hulvat, J. W. Lomasney, S. I. Stupp, *Nano Lett.*, 2006, **9**, 2086–2090.
74 R. Brayner, H. Barberousse, M. Hemadi, C. Djedjat, C. Yepremian, T. Coradin, J. Livage, F. Fievet, A. Couté, *J. Nanosci. Nanotech.*, 2007, **7**, 2696–2708.
75 D. Ghosh, Y. Lee, S. Thomas, A. G. Kohli, D. S. Yun, A. M. Belcher, K. A. Kelly, *Nature Nanotech.,* 2012, **7**, 677–682.
76 Y. J. Lee, H. Yi, W.-J. Kim, K. Kang, D. S. Yun, M. S. Strano, G. Ceder, A. M. Belcher, *Science*, 2009, **324**, 1051–1055.
77 Y. S. Nam, A. P. Magyar, D. Lee, J.-W. Kim, D. S. Yun, H. Park, T. S. Pollom, Jr, D. A. Weitz, A. M. Belcher, *Nature Nanotech.*, 2010, **5**, 340–344.
78 G. Liang, H. Ren, J. Rao, *Nature Chem.*, 2010, **2**, 54–60.
79 J. J. Gassensmith, E. Arunkumar, L. Barr, J. M. Baumes, K. M. DiVittorio, J. R. Johnson, B. C. Noll, B. D. Smith, *J. Am. Chem. Soc.*, 2007, **129**, 15054–15059.
80 See dedicate issue *Coord. Chem. Rev.*, 2009, **253** and refs therein.
81 See dedicate issue *Dalton Trans.*, 2011, **40** and refs therein.
82 For a very recent example see: S. Y.-L. Leung, W. H. Lam, V. W.-W. Yam, *Proc. Nat. Acad. Sci. USA*, 2013, **11**, 7986–7991.
83 V. W.-W. Yam, K. M.-C. Wong, N. Zhu, *J. Am. Chem. Soc.*, 2002, **124**, 6506–6507.
84 For a recent example see: X. Zhang, B. Cao, E. J. Valente, T. K. Hollis, *Organometallics*, 2013, **32**, 752–761.
85 Y. Tanaka, K. M.-C. Wong, V. W.-W. Yam, *Chem. Sci.*, 2012, **3**, 1185–1191.
86 L.-Y. Zhang, L.-J. Xu, X. Zhang, J.-Y. Wang, J. Li, Z.N. Chen, *Inorg. Chem.*, 2013, **52**, 5167–5175.
87 Y. Sun, K. Ye, H. Zhang, J. Zhang, L. Zhao, B. Li, G. Yang, B. Yang, Y. Wang, S.-W. Lai, C.-M. Che, *Angew. Chem.*, 2006, **118**, 5738–5741.
88 W. Zhang, W. Jin, T. Fukushima, N. Ishii, T. Aida, *Angew. Chem. Int. Ed.*, 2009, **48**, 4747–4750.
89 V. N. Kozhevnikov, B. Donnio, D. W. Bruce, *Angew. Chem. Int. Ed.*, 2008, **47**, 6286–6289.
90 Y. Li, E. S.-H. Lam, A. Y.-Y. Tam, K. M.-C. Wong, W. H. Lam, L. Wu, V. W.-W. Yam, *Chem. Eur. J.*, 2013, **19**, 9987–9994.
91 N. K. Allampally, C. A. Strassert, L. De Cola, *Dalton Trans.*, 2012, **41**, 13132–13137.
92 C. A. Strassert, C.-H. Chien, M. D. Galvez Lopez, D. Kourkoulos, D. Hertel, K. Meerholz, L. De Cola, *Angew. Chem. Int. Ed.*, 2011, **50**, 946–950.
93 S. Y.-L. Leung, V. W.-W. Yam, *Chem. Sci.*, 2013, **4**, 4228–4234.
94 M.-Y. Yuen, V. A. L. Roy, W. L., S. C. F. Kui, G. S. M. Tong, M.-H. So, S. S.-Y. Chui, M. Muccini, J. Q. Ning, S. J. Xu, C.-M. Che, *Angew. Chem. Int. Ed.*, 2008, **47**, 9895–9899.
95 M. C.-L. Yeung, V. W.-W. Yam, *Chem. Sci.*, 2013, **4**, 2928–2935.
96 V. W.-W. Yam, K. H.-Y. Chan, K. M.-C. Wong, N. Zhu, *Chem. Eur. J.*, 2005, **11**, 4535–4543.
97 C.-M. Che, C.-F. Chow, M.-Y. Yuen, V. A. L. Roy, W. Lu, Y. Chen, S. S.-Y. Chui, N. Zhu, *Chem. Sci.*, 2011, **2**, 216–222.
98 C. Yu, K. H.-Y. Chan, K. M.-C. Wong, V. W.-W. Yam, *Proc. Nat. Acad. Sci. USA*, 2006, **103**, 19652–19657.
99 C. Yu, K. H.-Y. Chan, K. M.-C. Wong, V. W.-W. Yam, *Chem. Eur. J.*, 2008, **14**, 4577–4584.
100 K. M.-C. Wong, V. W.-W. Yam, *Acc. Chem. Res.*, **44**, 2011, 424–434.
101 O. J. Staceya, S. J. A. Pope, *RSC Adv.,* 2013, **3**, 25550–25564.
102 P. I. Djurovich, D. Murphy, M. E. Thompson, B. Hernandez, R. Gao, P. L. Hunt, M. Selke, *Dalton Trans*., 2007, **34**, 3763–3770.
103 M. Mauro, G. De Paoli, M. Otter, D. Donghi, G. D'Alfonso, L. De Cola, *Dalton Trans.*, 2011, **40**, 12106–12116.
104 A. Ruggi, M. Mauro, F. Polo, D. N. Reinhoudt, L. De Cola, A. H. Velders, *Eur. J. Inorg. Chem.*, 2012, 1025–1037.
105 A. W.-T. Choi, M.-W. Louie, S. P.-Y. Li, H.-W. Liu, B. T.-N. Chan, T. C.-Y. Lam, A. C.-C. Lin, S.-H. Cheng, K. K.-W. Lo, *Inorg. Chem.*, 2012, **51**, 13289–13302.
106 M. P. Coogan, V. Fernández-Moreira, J. B. Hess, S. J. A. Pope, C. Williams, *New J. Chem.*, 2009, **33**, 1094–1099
107 D. Maggioni, F. Fenili, L. D'Alfonso, D. Donghi, M. Panigati, I. Zanoni, R. Marzi, A. Manfredi, P. Ferruti, G. D'Alfonso, E. Ranucci, *Inorg. Chem.*, 2012, **51**, 12776–12788.
108 M. Mauro, A. Aliprandi, C. Cebrián, D. Wang, C. Kübel, L. De Cola, *manuscript submitted.*
109 S.-W. Lai, Y. Liu, D. Zhang, B. Wang, C.-N. Lok, C.-M. Che, M. Selke, *Photochem. Photobio.*, 2010, **86,** 1414–1420.
110 T. Zou, C.-N. Lok, Y. M. E. Funga, C.-M. Che*, Chem. Commun.*, 2013, **49**, 5423–5425.
111 F. Arnesano, G. Natile, *Coord. Chem. Rev.,* 2009, **253**, 2070–2081.
112 X. Mou, Y. Wu, S. Liu, M. Shi, X. Liu, C. Wang, S. Sun, Q. Zhao, X. Zhoua, W. Huang, *J. Mater. Chem.*, 2011, **21**, 13951–13962.
113 N. Kumari, B. K. Maurya, R. K. Koiri, S. K. Trigun, S. Saripella, M. P. Coogan, L. Mishra, *Med. Chem. Commun.*, 2011, **2**, 1208–1216.
114 S. W. Botchway, M. Charnley, J. W. Haycock, A. W. Parker, D. L. Rochester, J. A. Weinstein, J. A. G. Williams, *Proc. Nat. Acad. Sci. USA*, 2008, **105**, 16071–16076.
115 E. Baggaley, S. W. Botchway, J. W. Haycock, H. Morris, I. V. Sazanovich, J. A. G. Williams, J. A. Weinstein, *Chem. Sci.*, 2014, doi: 10.1039/c3sc51875b.
116 R. McGuire, M. C. McGuire, D. R. McMillin, *Coord. Chem. Rev.*, 2010, **254**, 2574–2583.
117 J. A. G. Williams, *Coord. Chem. Rev.*, 2008, **252**, 2596–2611.
118 S.-W. Lai, C.-M. Che, *Top. Curr. Chem.*, 2004, 241, 27–63.
119 G. S.-M. Tong, C.-M. Che *Chem. Eur. J.*, 2009, **15**, 7225–7237.
120 C.-K. Koo, K.-L. Wong, C. W.-Y. Man, Y.-W. Lam, L. K.-Y. So, H.-L. Tam, S.-W. Tsao, K.-W. Cheah, K.-C. Lau, Y.-Y.

Yang, J.-C. Chen, M. H.-W. Lam, *Inorg. Chem.*, 2009, **48**, 872–878.

121 H. Andersson, T. Baechi, M. Hoechl, C. Richter, *J. Microscopy*, 1998, **191**, 1–7.

122 J. E. Aubin, *J. Histochem. Cytochem.*, 1979, **27**, 36–43.

123 C.-K. Koo, K.-L. Wong, C. W.-Y. Man, H.-L. Tam, S.-W. Tsao, K.-W. Cheah, M. H.-W. Lam, *Inorg. Chem*., 2009, **48**, 7501–7503.

124 C.-K. Koo, L. K.-Y. So, K.-L. Wong, Y.-M. Ho, Y.-W. Lam, M. H.-W. Lam, K.-W. Cheah, C. C.-W. Cheng, W.-M. Kwok, *Chem. Eur. J.*, 2010, **16**, 3942–3950.

125 M. P. Murphy, R. A. Smith, *Annu. Rev. Pharmacol. Toxicol*., 2007, **47**, 629–656.

126 K. M. Robinson, M. S. Janes, M. Pehar, J. S. Monette, M. F. Ross, T. M. Hagen, M. P. Murphy, J. S. Beckman *Proc. Nat. Acad. Sci. USA*, 2006, **103**, 15038–15043.

127 P. Wu, E. L.-M. Wong, D.-L. Ma, G. S.-M. Tong, K.-M. Ng, C.-M. Che, *Chem. Eur. J.*, 2009, **15**, 3652–3656.

128 R. W.-Y. Sun, A. L.-F. Chow, X.-H. Li, J. J. Yan, S. S.-Y. Chui, C.-M. Che, *Chem. Sci.*, 2011, **2**, 728–736.

129 X.-S. Xiao, W.-L. Kwong, X. Guan, C. Yang, W. Lu, C.-M. Che, *Chem. Eur. J.*, 2013, **19**, 9457–9462.

130 J. F. Zhang, C. S. Lima, B. R. Choa, J. S. Kim, *Talanta*, 2010, **83**, 658–662.

131 S. Wu, C. Zhu, C. Zhang, Z. Yu, W. He, Y. He, Y. Li, J. Wang, Z. Guo, *Inorg. Chem.*, 2011, **50**, 11847−11849.

132 R. R. de Haas, R. P. M. van Gijswijk, E. B. van der Tol, H. J. M. A. A. Zijlmans, T. Bakker-Schut, J. Bonnet, N. P. Verwoerd, H. J. Tanke, *J. Hystochem. Cytochem.,* 1997, **45**, 1279–1292.

133 R. R. de Haas, R. P. M. van Gijlswijk, E. B. van der Tol, J. Veuskens, H. E. van Gijssel, R. B. Tijdens, J. Bonnet, N. P. Verwoerd, H. J. Tanke, *J. Hystochem. Cytochem.,* 1999, **47**, 183–196.

134 R. Kumar, T. Y. Ohulchanskyy, I. Roy, S. K. Gupta, C. Borek, M. E. Thompson, P. N. Prasad, *ACS Appl. Mater. Inter.*, 2009, **1**, 1474–1481.

135 D. Domínguez-Gutiérrez, G. De Paoli, A. Guerrero-Martínez, G. Ginocchietti, D. Ebeling, E. Eiser, L. De Cola, C. J. Elsevier, *J. Mater. Chem.*, 2008, **18**, 2762–2768.

136 S. Liu, H. Sun, Y. Ma, S. Ye, X. Liu, X. Zhou, X. Mou, L. Wang, Q. Zhao, W. Huang, *J. Mater. Chem.*, 2012, **22**, 22167–22173.

137 W. Lu, C. W. Chan, N. Zhu, C.-M. Che, C. Li, Z. Hui, *J. Am. Chem. Soc.*, 2004, **126**, 7639–7651.

138 S.-W. Lai, M. C.-W. Chan, T.-C. Cheung, S.-M. Peng, C.-M. Che, *Inorg. Chem.*, 1999, **38**, 4046–4055.

139 Y. Hong, J. W. Y. Lam, B. Z. Tang, *Chem. Soc. Rev.*, 2011, **40**, 5361–5388 and refs therein.

140 Q. Zhao, L. Li, F. Li, M. Yu, Z. Liu, T. Yi, C. Huang, *Chem. Commun.*, 2008, 685–687.

141 E. Quartapelle Procopio, M. Mauro, M. Panigati, D. Donghi, P. Mercandelli, A. Sironi, G. D'Alfonso, L. De Cola, *J. Am. Chem. Soc.*, 2010, **132**, 14397–14399.

142 L. De Cola, M. Mauro, S. Kehr, C. A. Strassert, PCT Int. Pat. Appl. WO2012117082.

143 H. L. Yale, *J. Med. Chem.*, 1958, **1**, 121–133.

144 S. Purser, P. R. Moore, S. Swallow, V. Gouverneur, *Chem. Soc. Rev.*, 2008, **37**, 320–330.

145 C. Y.-S. Chung, S. P.-Y. Li, M.-W. Louie, K. K.-W. Lob, V. W.-W. Yam, *Chem. Sci.*, 2013, **4**, 2453–2462.

 

**Chart 1.** Chemical structures of the bidentate platinum(II) complexes discussed in this review.

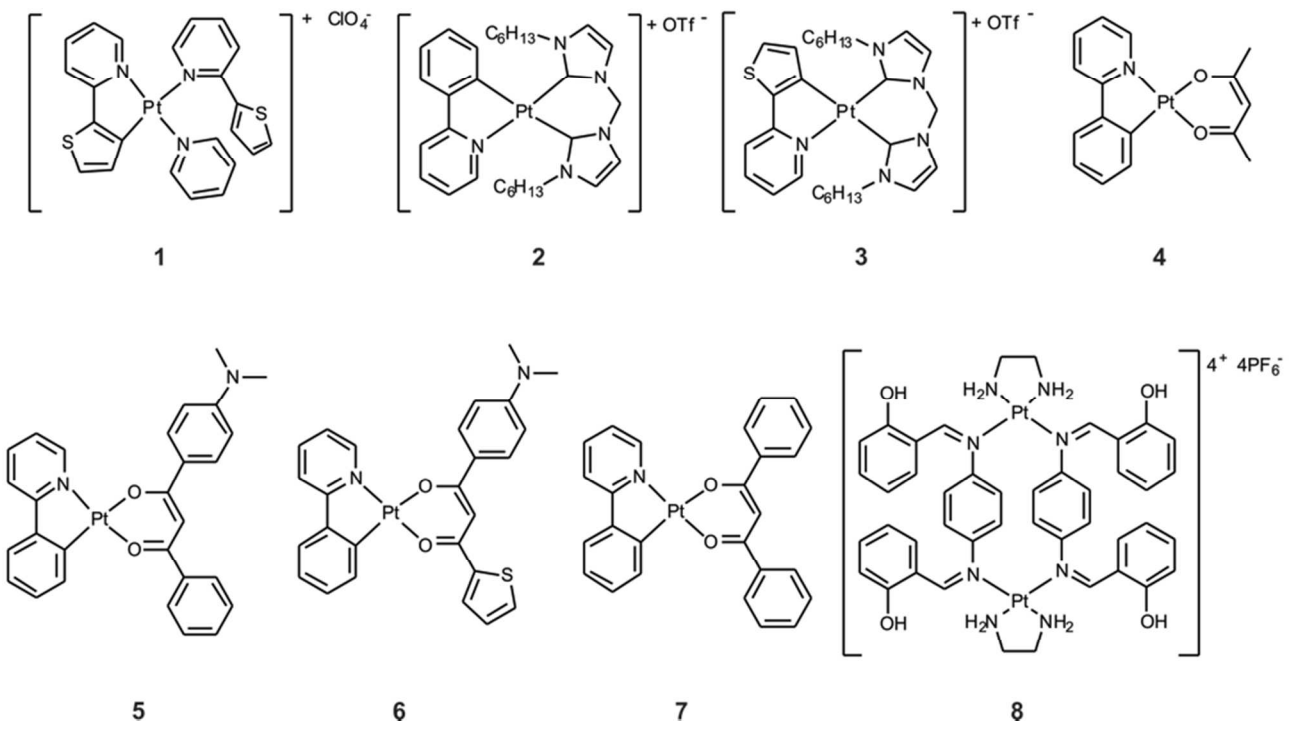

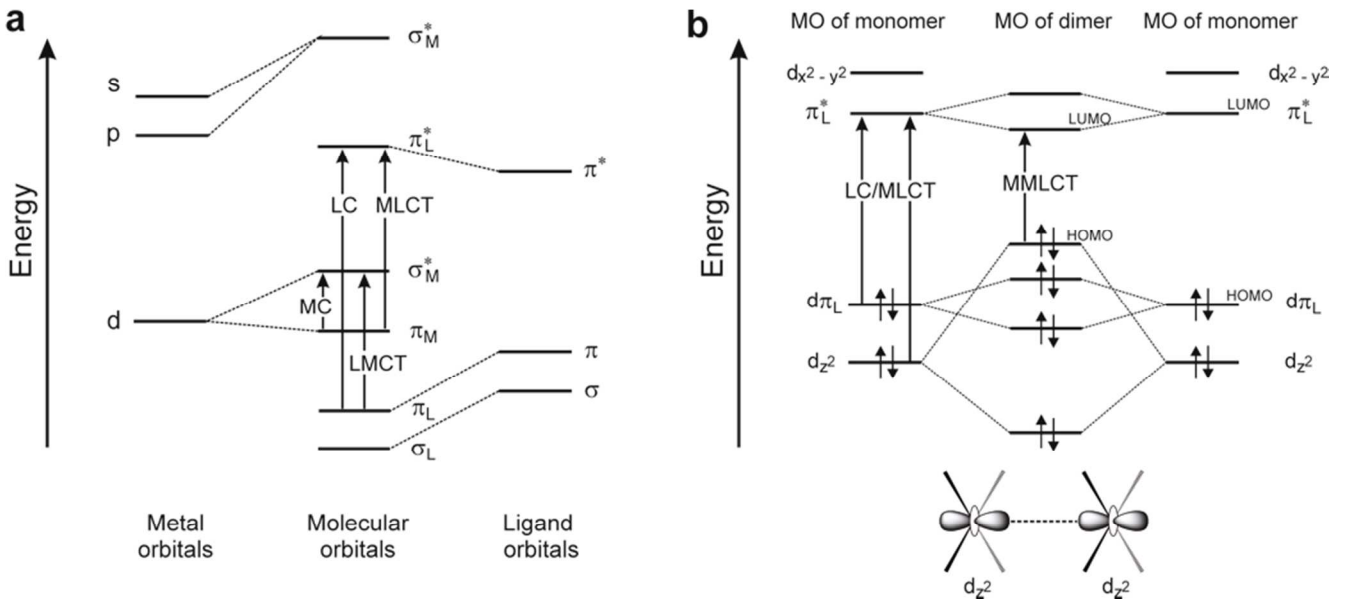


**Fig. 1**. (a) Simplified MO diagram for a generic transition metal complex and relative spectroscopic excitation transitions. (b) Simplified MO diagram of two interacting square-planar platinum(II) complexes, showing the intermolecular $d_z^2$ orbital overlap in the ground-state and its influence on energy of the MO energy level.

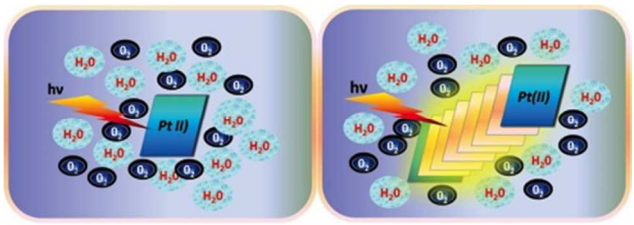


**Fig. 2**. Schematic representation of the deactivation of a platinum complex by the environment (left) and the rigidochromic and shielding effect imparted by the aggregation, resulting in the emission enhancement (right).

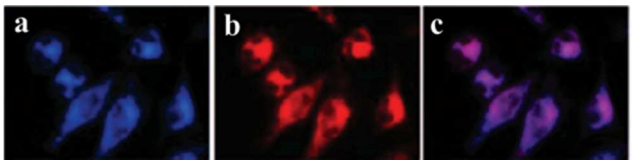


**Fig. 3.** (a) Fluorescent confocal microscopy images of HeLa cells stained with complex **2**. (b) ER Tracker® stain. (c) Merged image showing the distribution of complex **2** inside the ER domains. Images were recorded upon excitation at 340 nm and 546 nm for complex **2** and ER Tracker®, respectively. Adapted from Ref. 110.

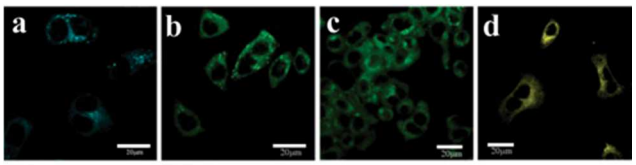


**Fig. 4.** Fluorescence microscopy images of complex **4** (a), **5** (b), **6** (c) and **7** (d) inside HeLa cells which was incubated with 10 μM of complex **4**–**7** in DMSO/PBS for 30 minutes at 37 ºC. Images were recorded upon excitation at 405 nm. Scale bar = 20 μm. Adapted from Ref. 112.

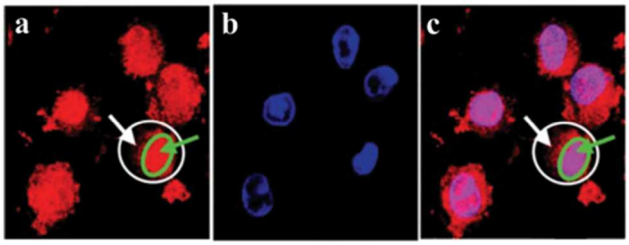


**Fig. 5.** (a) Fluorescence microscopy images of internalization and localization of complex **8** inside HeLa cells. (b) Selective nuclear staining with Hoechst 33342. (c) Merged image (a) and (b). Green circles in (a) and (c) show the nuclear boundary and white ovals show cell boundaries. Green arrows show the intense localization of complex **8** inside the cell nucleus, while white arrows in window (a) and (c) point to the region with lower concentration of complex **8**. Images were recorded upon excitation at 405 nm and 488 nm, respectively. Adapted from Ref. 113.

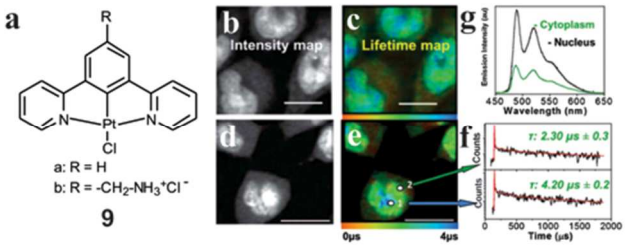


**Fig. 6.** (a) Chemical structure of the N^C^N platinum complexes **9a–b**. (b) Time resolved confocal imaging of live cells and sensitivity to the micro-environment. TP-TREM of CHO-K1 cells labeled with **9b** (b) and (c) and **9a** (d–g) under 760 nm, ~120 fs two-photon excitation. (b) and (d) Intensity images reconstructed by integrating total emission intensity pixel-per-pixel. (c) Lifetime map corresponding to (b). (e) Lifetime map corresponding to (d). (f) Kinetic traces from pixels 1 and 2 on (e), red line corresponds to the lifetime fitting of the main component [pixel symbol magnified for clarity]. (g) Emission spectra recorded from nucleus and cytoplasm (e). Adapted from Ref. 115.

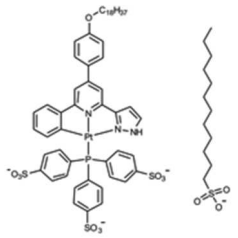


**Fig. 7.** Chemical structure of the C^N^N platinum complex **11** (left) and comparison with the SDS surfactant (right).

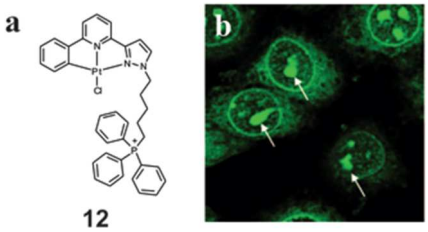


**Fig. 8.** Chemical formula of complex **12** and fluorescence microscopy image of HeLa cells stained with **12**, showing the labelling of the cellular nuclear domains (arrows). The image was recorded upon the excitation at 405 nm. Adapted with permission from Ref. 124.

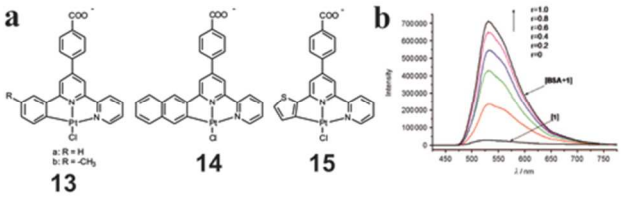


**Fig. 9.** (a) Chemical formulas of complexes **13**–**15**. (b) Changes in the emission spectra of complex **13a** upon addition of different concentration of BSA. Adapted with permission from Ref. 127.

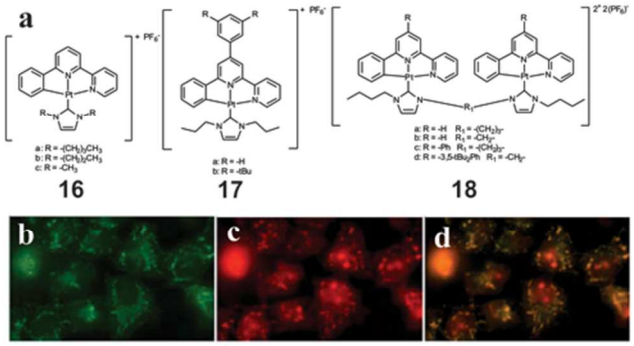


**Fig. 10.** (a) Chemical formulas of complexes **16**–**18**. (b) Fluorescent microscopic examination of HeLa cells incubated with **16a** and co-incubated with MitoTracker™ (c). (d) Merged image showing that the majority of **16a** can be co-localized with MitoTracker™. Adapted from Ref. 128.

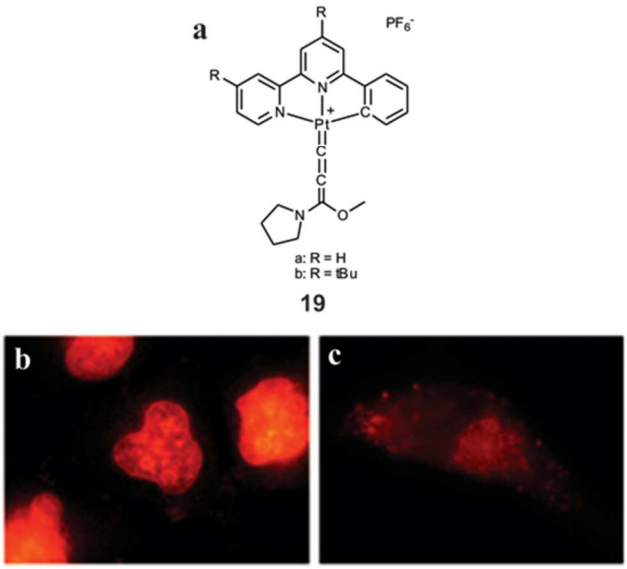


**Fig. 11.** (a) Chemical formulas of the allenylidene platinum complexes **19a**–**b**. (b) and (c) Cellular imaging of **19a** and **19b** in viable HeLa cells, observed under fluorescence microscope revealing the subcellular localization of **19a** and **19b**, respectively. Adapted with permission from Ref. 129.

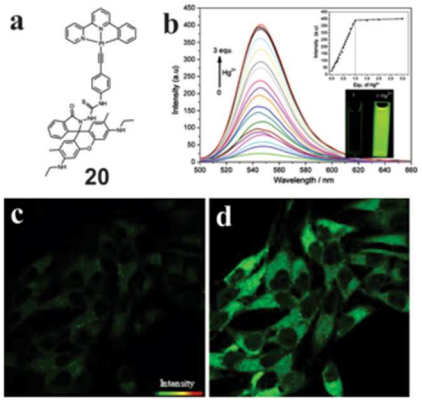


**Fig. 12.** (a) Chemical formula of complex **20**. (b) Changes in the emission spectra of **20** in $CH_3CN$/HEPES buffer (20 mM, pH 7.0, $^{v}/_{v}$ 50/50) upon addition of $Hg^{2+}$ ($\lambda_{exc}$ = 490 nm). (c) and (d) TPM image of HeLa cells labeled with **20** before and after addition of $Hg^{2+}$, respectively. Adapted with permission from Ref. 130.

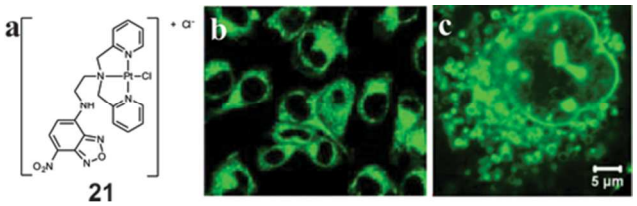


**Fig. 13.** (a) Chemical structure of compound **21**. (b) Fluorescence microscopy image of MCF-7 cells stained with the free ligand after 20 minutes incubation. (c) Fluorescence microscopy image of MCF-7 cells stained with the complex **21**, after 5 hours incubation bright vacuoles are observed. Adapted with permission from Ref. 131. Copyright 2011 American Chemical Society

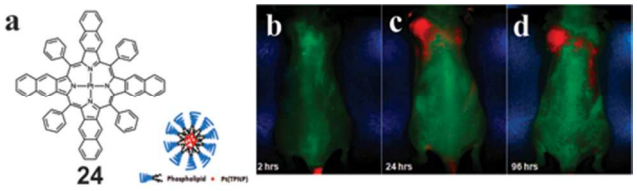


**Figure 14.** (a) Chemical structure of the porphyrinic platinum complex **24**. *In vivo* phospholuminescence (PL) imaging experiment in xenografted nude mice showing the distribution of the encapsulated platinum porphyrin complex **24** into micelles after different time delay upon injection (b–d). Images show the accumulation of **24** (red color) at the tail two hours post injection while after 24 and 96 hours the complexes were found at the tumor sites. Images were recorded by Maestro GNIR FLEX fluorescence imaging system upon the excitation of xenon lamp at wavelength 650–700 nm. Adapted with permission from Ref. 134. Copyright 2009 American Chemical Society

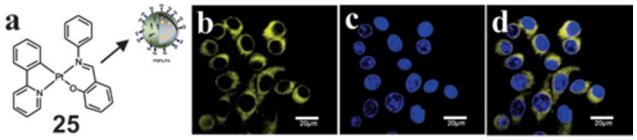


**Figure 15.** (a) Chemical formula of complex **25** and its encapsulation embedded into polyacrylamide-coated polystyrene. The particles are functionalized with folic acid. (b) Confocal luminescence images of living HeLa cells stained with the particles and (c) DAPI; (d) merged image (b) and (c). Adapted from Ref. 136.

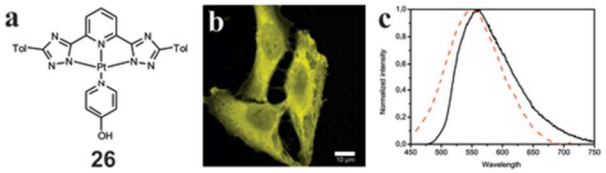


**Figure 16.** (a) Chemical formula of the complex **26**. (b) Microscopy images of internalization of complex **26** into HeLa cells. Cells were incubated for 4 hours with 50 μM of **26** in <1% DMSO in PBS. Images were taken upon excitation at 405 nm. (c) Comparison of the emission spectra of **26** in the cytoplasm (red trace) and in water :1%DMSO (black trace). Scale bar = 10 μm.

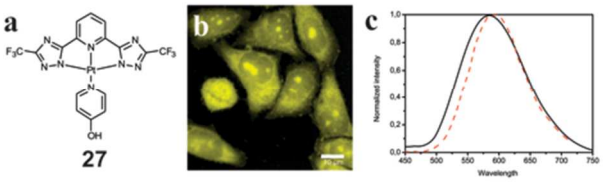


**Figure 17.** (a) Chemical formula of complex **27** and its internalization and confocal image (b) showing the presence of the complex as aggregates into the nucleus. (c) The emission inside the nucleus (red trace) is almost identical to that of the aggregates in 1% DMSO:$H_2O$ (black trace). Scale bar = 10 μm.

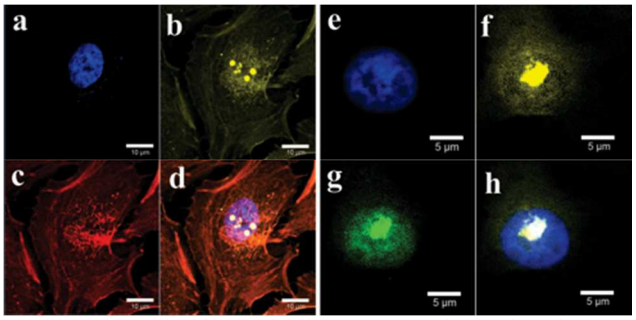


**Fig. 18**. Microscopy images of distribution of complex **27** inside HeLa cells. (a) DAPI stains nucleus (b) complex **27**, (c) Phalloidin Alexa Fluor® 568 stains actin inside cytoplasmic region, (d) overlay of (a), (b) and (c). The excitation wavelengths of DAPI, complex **27** and Phalloidin Alexa Fluor® 568 are 405 and 594 nm, respectively. Localization has been obtained as follows: (e) DAPI stains nucleus, (f) complex **27**, (g) SYTO® RNASelect™ Green Fluorescent Cell Stain stains nucleoli, (h) overlay of (a), (b), (c). Co-localisation experiments show a very bright aggregate signal (f) coming from inside the nuclear region (e) is distributed inside nucleoli (g). The excitation wavelengths of DAPI, complex **27** and SYTO® RNASelect™ Green Fluorescent Cell Stain are 405 and 488 nm, respectively. Scale bar = 10 and 5 μm for (a)–(d) and (e)–(h), respectively.

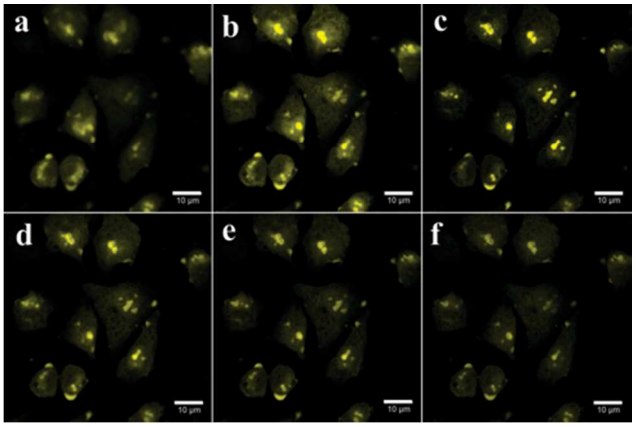


**Figure 19**. Fluorescence images of internalization of complex **27** inside HeLa cells upon excitation at 355 nm (a), 405 nm (b), 458 nm (c), 488 nm (d), 514 nm (e), and 543 nm (f). Scale bar = 10 μm.

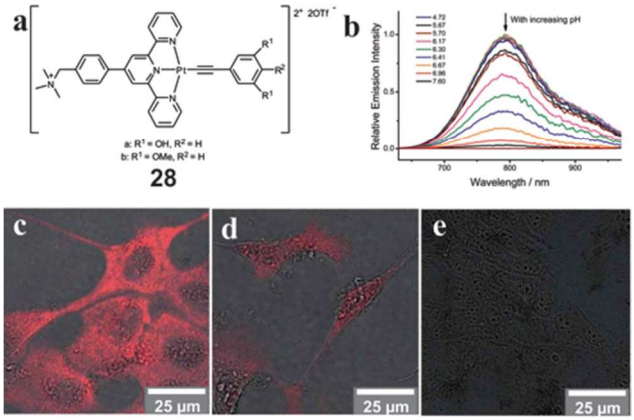


**Figure 20**. (a) Chemical structure of complexes **28**. (b) Emission spectra of complex **28a** (200 μM) in aqueous solution (50 mM NaCl) at various pH values (λex = 480 nm). (c–e) Confocal microscopy images of fixed MDCK cells incubated with 20 μM of complex **28a** for 1 hour followed by incubation with buffer solutions at different pH: pH 5.72 (c), pH 6.75 (d) and pH 7.80 (e). $\lambda_{ex}$ = 488 nm. Adapted from Ref. 145.

Journal Name RSCPublishing

ARTICLE

**Table 1.** Spectroscopy data of series of Pt(II) complexes together with preferential cellular localization and viability.

| Complex | Structure | $\lambda_{em}$(nm) | Φ | τ [μs] | Incubation conditions | viability $IC_{50}$ | Cell co--localization | Ref |
|---|---|---|---|---|---|---|---|---|
| **1** | 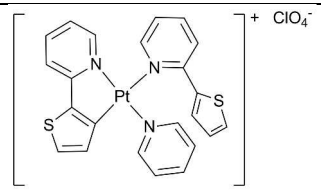 | 464, 553, 596 (TBS); 602 ($CH_3CN$) | 0.38 (deg) | 0.33 (air) 24 ($N_2$) | 5 μM, 1 hour, 37°C, MEM + 10% FBS | 6.12 μM (in the dark) 1.78 μM (under light irradiation) | Mitochondria and nucleous | 110 |
| **2** | 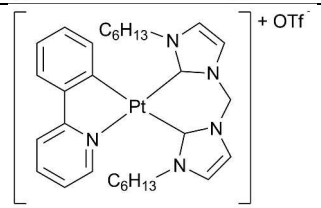 | 485–517 ($CH_2Cl_2$) | 0.051 (deg) | 1.7 | 5 μM, 10 minutes, | 0.45-1.59 μM | Endoplasmic reticulum | 111 |
| **3** | 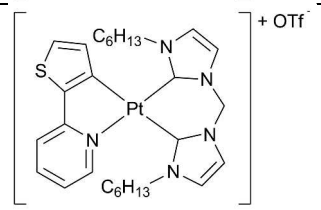 | 560–604 ($CH_2Cl_2$) | 0.24 (deg) | 29.2 | 5 μM, 10 minutes, | 2.75-44.3 μM | Endoplasmic reticulum | 111 |
| **4** | 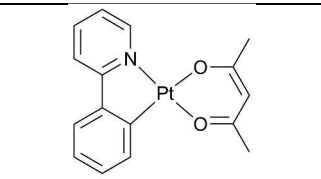 | 493,528 (DMSO/PBS (1/99, v/v)) | 0.11 ($CH_2Cl_2$) | | 10 μM, 30 minutes, 37°C, DMSO/PBS (1/99, v/v) | >80% viability | Cytoplasm | 113 |

| | | | | | | | | |
|---|---|---|---|---|---|---|---|---|
| **5** | 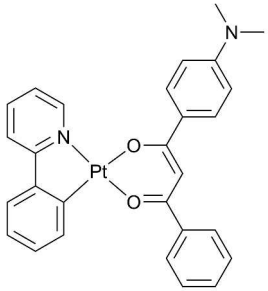 | 522 (DMSO/PBS (1/99)) | 0.044 ($CH_2Cl_2$) | | 10 μM, 30 minutes, 37°C, DMSO/PBS (1/99, v/v) | >85% viability | Cytoplasm | 113 |
| **6** | 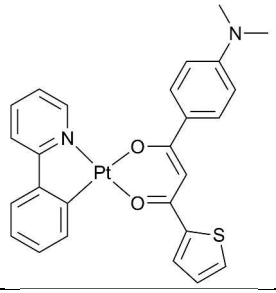 | 532 (DMSO/PBS (1/99)) | 0.018 ($CH_2Cl_2$) | | 10 μM, 30 minutes, 37°C, DMSO/PBS (1/99, v/v) | ≈90%viability | Cytoplasm | 113 |
| **7** | 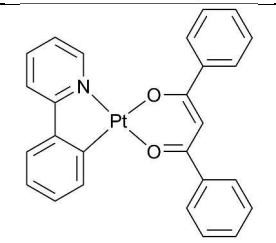 | 545 (DMSO/PBS (1/99)) | 0.086 ($CH_2Cl_2$) | | 10 μM, 30 minutes, 37°C, DMSO/PBS (1/99, v/v) | ≈ 85%viability | Cytoplasm | 113 |
| **8** | 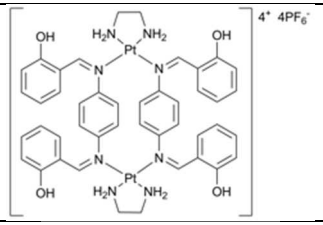 | ~500 (DMSO) | | 0.0043 | 20 μM, 30 minutes, PBS | 11.5 μM | Nucleus | 114 |
| **9** | 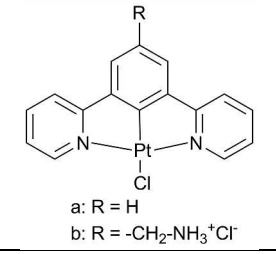 a: R = H b: R = -$CH_2$-$NH_3^+Cl^-$ | 491, 524, 562 ($H_2O$ and $CH_2Cl_2$) | 0.6 (deg) 0.039 (air) | 7.2 (deg) 0.5(air) | 100 μM, 5 minutes, PBS | no significant decrease in metabolic activity | Nucleus | 115, 116 |

| | | | | | | | | |
|---|---|---|---|---|---|---|---|---|
| **10** | 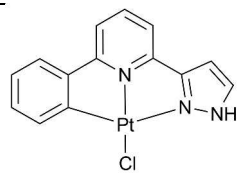 | 500-520 (DMF, HEPES buffer/DMSO 95/5, v/v) | 0.09 (DMF), 0.1 (HEPES buffer/DMSO 95/5, v/v) | 0.57 (DMF), 1.46 (HEPES buffer/DMSO 95/5, v/v) | 1 μg/mL, 5 minutes, culture medium | no significant decrease in metabolic activity | Cytoplasm | 121 |
| **11** | 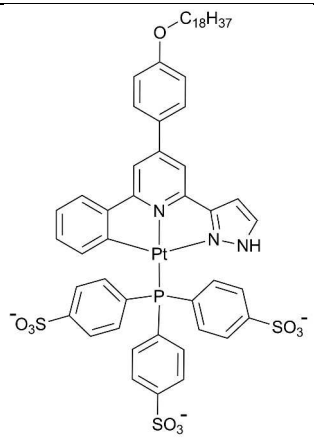 | 528 (HEPES buffer) | 0.3 (HEPES buffer) | 1.95 | 1 μg/mL in cell culture medium | 90% viability | Plasma membrane | 124 |
| **12** | 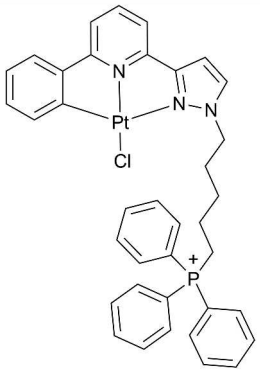 | 510 ($CH_3CN$) | 0.10 ($CH_3CN$) | 0.36 ($CH_3CN$) | 0.1-1 mM, 15 minutes | Significant cell death | Nucleoli | 125 |
| **13** | 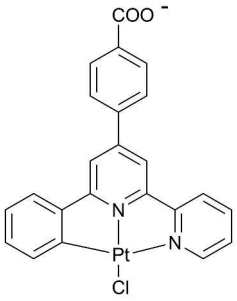 | 563 ($H_2O$) | 0.01 | <0.1 | 5 μM, 24 hours | 80 μM | Authors suggested the sublocalization inside endoplasmic reticulum and golgi apparatus | 128 |

| | | | | | | | | |
|---|---|---|---|---|---|---|---|---|
| **16a** | 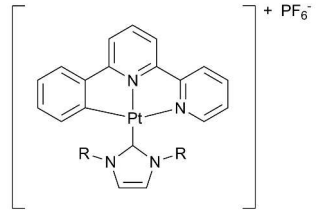 | 545 ($CH_3CN$) | 0.23 ($CH_3CN$) | 1.2 ($CH_3CN$) | 1 μM, 1 hour | 0.057μM | Mitochondria | 129 |
| **19** | 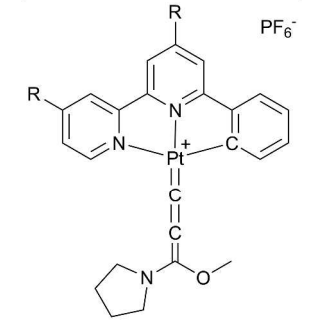 a: R = H b: R = tBu | a: 542 ($CH_2Cl_2$, deg), b: 530 ($CH_2Cl_2$, deg) | a: 0.34 ($CH_2Cl_2$, deg) b: 0.63 ($CH_2Cl_2$, deg) | a: 3.9 ($CH_2Cl_2$, deg) b: 4.5 ($CH_2Cl_2$, deg) | 20 μM, 37 °C, 2 hours, Tris-HCl (5 mm) buffer | a: 5.8 μM b: 9 μM | a: Nucleus b: Cytoplasm | 130 |
| **20** | 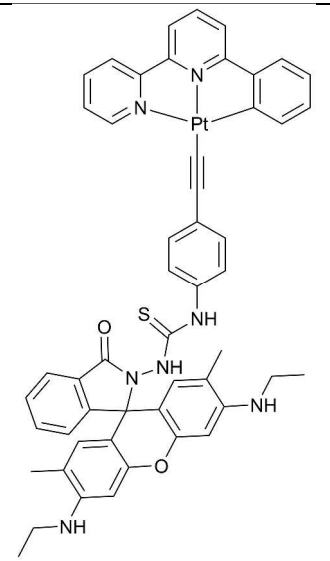 | 545 ($CH_3CN$) | | | 2 μM, 37°C 20 minutes, DMEM | | | 131 |

| | | | | | | | | |
|---|---|---|---|---|---|---|---|---|
| **21** | 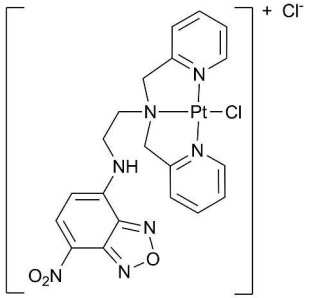 | 546 (PBS 0.3% DMSO) | | | MCF-7 cell, 10 μM, 25°C, 0.5-5 hours, PBS, <1% DMSO | 45.9 μM | Mitochondria and nucleus | 132 |
| **22** | 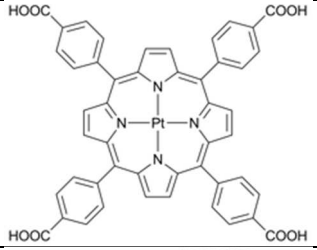 | 675 (PB pH 8) | 0.12 | 28 | | | Coniugated with vidin, streptavidin, neutravidin, and antibodies | 133, 134 |
| **23** | 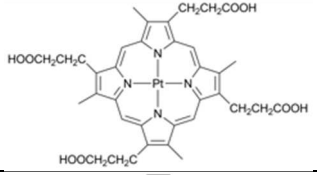 | 650 (PB pH 8) | 0.23 | 52 | 10 μg/ml in TNB | | Coniugated with avidin, streptavidin, neutravidin, and antibodies | 133, 134 |
| **24** | 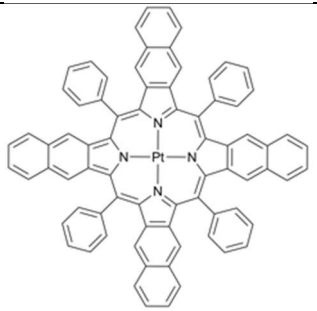 | 903 ($CHCl_3$) | 0.01 ($CHCl_3$)<br>0.22 (Toluene, deg) | 1.3 μs ($CHCl_3$) | Polimeric particle ~100 nm size, 30 μg/ml (water with 5% glucose), in vivo animal imaging | 90 % (0.225 μg/ml) | Highly specific accumulation into tumor site | 135 |
| **25** | 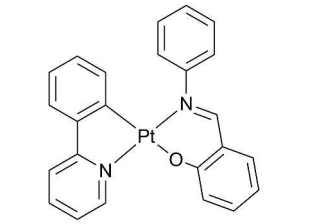 | 550 ($H_2O$/THF) | | | 70 nm polymeric nanoparticle 0.2 mg/mL, 37°C, 30 minutes | >95% | Cytoplasm | 137 |

| | | | | | | | | |
|---|---|---|---|---|---|---|---|---|
| **26** | 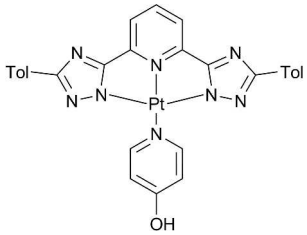 | 560 ($H_2O$/1% DMSO) | | | 50 μM in less than 1% DMSO in PBS, 37°C, 4 hours | | Cytoplasm | 143 |
| **27** | 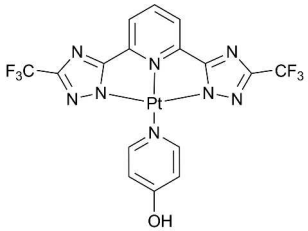 | 585 ($H_2O$/1% DMSO) | | 0.9 | 50 μM in less than 1% DMSO in PBS, 37°C, 4 hours | | Cytoplasm, nucleoli | 143 |
| **28** | 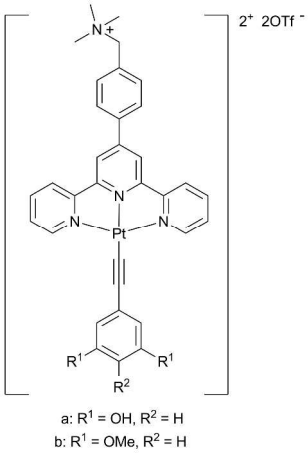 a: $R^1$ = OH, $R^2$ = H b: $R^1$ = OMe, $R^2$ = H | a: 582 ($CH_3CN/CH_3OH$, 5/1, v/v), 788 (pH 7 aqueous solution), 795 (pH 3 aqueous solution) b: 634 (DMF), 654 ($CH_3CN/CH_3OH$, 5/1, v/v), 788 (pH 3,7, and 10 aqueous solution) | | a: 0.2 ($CH_3CN/CH_3OH$, 5/1, v/v), 0.1 (pH 3, 7 aqueous solution), b: 0.1 ($CH_3CN/CH_3OH$, 5/1, v/v), and DMF), <0.1 (pH 3,7, and 10 aqueous solution) | MDCK cells, 20 μM, 37°C, 1 hour, phenol red-free DMEM, 0.2% DMSO | a: 97% viability | a: lysosomes b: diffused | 144 |

TBS = Tris Buffer Solution, MEM = Minimum Essential Medium, DMEM = Dulbecco's Modified Eagle Medium, FBS = Fetal Bovine Serum

PB = 50 μM Phosphate buffer, TNB = Tris-NaCl-blocking buffer, deg = degassed. HeLa cells were employed unless specified

Journal Name RSCPublishing

ARTICLE

## Biographies

**Prof. Luisa De Cola** is a full Professor at the University of Strasbourg, Institut de Science et d'Ingénierie Supramoléculaires (I.S.I.S.), on the AXA chair Supramolecular and biomaterials chemistry. She is also associated scientist at the Karlsruhe Institute of Technology, KIT, (Germany) in the Nanotechnology Institute. Her research focuses on (electro)luminescent materials for diagnostics and devices, and nanomaterials for imaging and medical applications. She studied chemistry at the University of Messina, Italy and after a post-doc at the Virginia Commonwealth University, USA she moved back to Italy at the CNR in Bologna to work with Prof. V. Balzani. She has received several awards, and recently the ERC advanced grant (2009), the IUPAC award as one of the Distinguished Women in Chemistry and Chemical Engineering (2011) and the Gutenberg Chair award (2012). She is a member of the Academia Europeae.

**Dr. Matteo Mauro** obtained his B.Sc. *cum laude* in Chemistry at the University of Bari (Italy) in 2004 and his M.Sc. (2006) and Ph.D. (2009) degree in Chemical Sciences at the University of Milano (Italy) under the supervision of Prof. G. D'Alfonso. After postdoctoral experiences at the University of Münster, Germany, since 2012 he has been appointed as Assistant Professor at the University of Strasbourg, Institut de Science et d'Ingénierie Supramoléculaires (I.S.I.S.), in the group of Prof. L. De Cola. To date, he has been awarded the Eni Award "debut research prize" (2010), Alexander von Humboldt fellowship (2011), and University of Strasbourg Institute for Advanced Studies (USIAS) fellowship (2013). His current research focuses on self-assembling (electro)-luminescent transition metal complexes and their application, as well as light-driven smart materials for soft robotics.

**Alessandro Aliprandi** received his master degree in Chemistry from the University of Ferrara in 2010 under the supervision of Prof. C.A. Bignozzi. After one year of fellowship in the same group, he joined Prof. Luisa De Cola's group as a PhD candidate at the University of Strasbourg, at the Institut de Science et d'Ingénierie Supramoléculaires (I.S.I.S.). His research focuses on self-assembly of luminescent transition metal complexes and bio-imaging.

**Dedy Septiadi** attended the Institut Teknologi Sepuluh Nopember (Indonesia) for his undergraduate and graduated in engineering physics with specialization in photonics in 2010 under the supervision of Dr. Nasution. He was then awarded an Erasmus Mundus master scholarship in molecular nano- and bio-photonics. He joined the Cavendish Laboratory at the University of Cambridge where he worked 6 months for his master thesis (2012) in the group of Dr. Mahajan. Starting from October

2012, he joined as PhD candidate Prof. De Cola's group to work in bio-imaging based on metal complexes and nanomaterial-cell interaction.

**Dr. Nermin Seda Kehr** studied chemistry at the Middle East Technical University in Ankara (Turkey) and did her PhD work with Prof. Dieter Hoppe at the University of Münster (Germany). After postdoctoral research with Prof. Bart Jan Ravoo, she joined the group of Prof. Luisa De Cola (Germany, France) to build up her own research. Currently she is connected to the group of Prof. Hans-Joachim Galla (Biochemistry, Münster) and is working on her habilitation. Her research interests are hybrid nanoparticles, chiral hydrogels, nanocomposite hydrogels and their applications in biotechnologies.

Journal Name RSCPublishing

## ARTICLE

TOC

Self-assembled luminescent structures based on platinum complexes. A new tool in bioimaging?